Accepted Manuscript

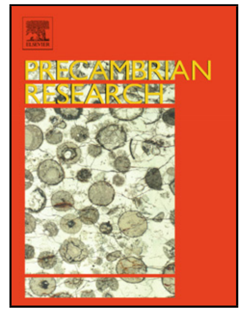

Title: Arctic Bay Formation, Borden Basin, Nunavut (Canada): basin evolution, black shale, and dissolved metal systematics in the Mesoproterozoic ocean

Authors: Elizabeth C. Turner, Balz S. Kamber

PII:	S0301-9268(12)00081-2
DOI:	doi:10.1016/j.precamres.2012.03.006
Reference:	PRECAM 3541

To appear in: *Precambrian Research*

Received date:	21-6-2011
Revised date:	9-3-2012
Accepted date:	14-3-2012

Please cite this article as: Turner, E.C., Kamber, B.S., Arctic Bay Formation, Borden Basin, Nunavut (Canada): basin evolution, black shale, and dissolved metal systematics in the Mesoproterozoic ocean, *Precambrian Research* (2010), doi:10.1016/j.precamres.2012.03.006

Highlights

- black shale of the rift-related late Mesoproterozoic Arctic Bay Fm. was deposited under a stratified oxygenated / anoxic water column
- metal enrichments were caused primarily by stripping from the water column and possibly enhanced by diagenetic redistribution into subtle carbonate-bearing layers
- concentrated venting was absent at the study location, but basin geochemistry was suitable for formation of SEDEX and polymetallic deposits
- U-Th-Pb whole-rock depositional age of the Arctic Bay Formation is 1092±59 Ma

Arctic Bay Formation, Borden Basin, Nunavut (Canada): basin evolution, black shale, and dissolved metal systematics in the Mesoproterozoic ocean

Elizabeth C. Turner[1,2] and Balz S. Kamber[2,3]

[2]Department of Earth Sciences, Laurentian University, Sudbury, Ontario, P3E 2C6, Canada

eturner@laurentian.ca[1]

[1] Corresponding author

[3] Now at: School of Natural Sciences, Trinity College Dublin, Dublin 2, Ireland

ABSTRACT

The Arctic Bay Formation (Nunavut, Canada) represents a late Mesoproterozoic muddy terrigenous ramp and contains >200 m of black shale. The formation was studied in order to decipher the tectonostratigraphic and geochemical evolution of the basin, address the origin of metal enrichment, and determine whether this frontier basin has the potential to host sedimentary-exhalative or polymetallic black shale deposits. Samples were analysed in the laboratory for major and trace elements, total organic carbon (TOC), 4-step loss-on-ignition (LOI), and Pb isotopes. Non-calcareous black shale exhibits neither Ce nor Y anomalies, reflecting euxinia in the lower water column, whereas slightly dolomitic black shale has both Ce and Y anomalies, reflecting the dolomite's probable origin as a precipitate in the upper water column. The stratigraphic distribution of the rare earth elements (REEs) indicates an evolving sediment provenance, and Pb isotopic data indicate that the source of clay in the black shale was dominated by weathered, juvenile, mantle-derived material. Base metals and redox-sensitive metals, expressed as enrichment ratios relative to conservative lithophile elements, are elevated and exhibit coherent covariations in the black shale. Enrichment in the redox-sensitive elements, such as Mo and U, correlates with dolomite content of the shale, rather than with organic C or Fe_{py}. From a deep-time ocean evolution perspective, this important observation suggests that enrichment in these metals cannot necessarily be attributed to metal incorporation at an interface between sediment and euxinic water. Instead, in Arctic Bay Formation black shale, the metals were either scavenged onto dolomite as it precipitated in the water column, or secondarily re-distributed within the sediment according to its dolomite content. The base metals that are concentrated in the black shale (e.g., Zn) were probably sourced from diffuse hydrothermal venting, and although there is no evidence at the studied location for a nearby point source of metals (vent), persistent bottom- water euxinia would have ensured the effective scavenging of any dissolved metals supplied, and so the basin has at the very minimum a hypothetical potential for SEDEX and polymetallic mineralisation. Whole-rock U-Th-Pb isotope analysis of black shale yielded a date of 1092±59 Ma, which is considered to be the Arctic Bay Formation's depositional age.

Keywords: black shale; geochemistry; Mesoproterozoic; Arctic Bay Formation; Borden Basin

1. INTRODUCTION

The Mesoproterozoic Borden Basin of the Canadian Arctic islands is an established mining district (carbonate-hosted Nanisivik deposit), but its tectonostratigraphic evolution is poorly understood, the basin's metal potential is underexplored, and many of its stratigraphic units have received only cursory attention. One of the stratigraphic units in this rift basin, the >1 km-thick Arctic Bay Formation, contains an impressive thickness of black shale about which little is known. Stratigraphic and geochemical data from the Arctic Bay Formation are used in this study as the basis for a discussion of the basin's tectonic and geochemical evolution, the distribution of metals as a function of stratigraphy, and the dynamics of dissolved redox-sensitive metals in Mesoproterozoic seawater. Such elements are critical to understanding the evolution of the Proterozoic atmosphere and ocean, but also provide a means of identifying possible horizons of economic interest in black shale basins. The Mesoproterozoic represents a global nadir in the temporal distribution of SEDEX deposits (Leach et al., 2010), a phenomenon that may be linked to the still poorly understood geochemical evolution of Earth's surface environments at the time.

2 .GEOLOGICAL SETTING

The Bylot Supergroup, a ~6 km-thick succession of Mesoproterozoic strata, was deposited in the Borden Basin, one of several ~1.2 Ga basins in the Canadian Arctic islands and northwestern Greenland (Figs. 1, 2A; Fahrig et al., 1981; Jackson and Iannelli, 1981). The Borden Basin consists of three "troughs" (Fig. 1), of which the Milne Inlet Graben (MIG) is both the largest, and the only one known to contain sulphide deposits (Nanisivik ore-body and other carbonate-hosted showings; Turner, 2011). The present study addresses the Arctic Bay Formation, a thick succession of fine-grained terrigenous clastic rocks in the lower Bylot Supergroup (Fig. 2). Strata of the basal Bylot Supergroup in the MIG locally reach prehnite-pumpellyite to greenschist facies, but strata higher in the succession remain unmetamorphosed (Jackson and Morgan, 1978; Galley et al., 1983; Dostal et al., 1989).

The MIG is a gently west-plunging trough with an abrupt northern margin and a more gradual southern margin (Fig. 1). The regional structure of the MIG (Jackson and Iannelli, 1981; Scott and deKemp, 1998) is dominated by pronounced northwest-trending intragraben and graben-margin fault systems. These faults accommodated both early extension and continued tectonic adjustments, strongly affected sedimentary facies distribution throughout MIG history, were the locus of deep-water carbonate mound growth of the Ikpiarjuk Formation (Turner, 2009), and were intermittently reactivated during the Phanerozoic (Jackson and Iannelli, 1981).

Rifting of the Archean basement gneiss (Rae Province) is recorded by a basal subaerial tholeiitic basalt (Nauyat Formation) that is related to the ~1.27 Ga Mackenzie igneous province (Fig. 2A; LeCheminant and Heaman, 1989). The basalt is overlain successively by the predominantly shallow-marine Adams Sound Formation quartz arenite and shale of the Arctic

Bay Formation (Jackson and Iannelli, 1981; Long and Turner, in press). The shale-dominated Arctic Bay Formation was described by Jackson and Iannelli (1981) as thinning northwestward, from ~770 m in most of the eastern Milne Inlet Graben to 180 m at Arctic Bay. The basal, gradational contact with the underlying Adams Sound Formation quartz arenite was interpreted as conformable. The upper contacts, with whichever of the three carbonate formations overlies it in any given location, are also conformable (Turner, 2009). Two paleogeographic zones were identified in the Arctic Bay Formation, with a boundary roughly at Milne Inlet (Jackson and Iannelli, 1981). The Arctic Bay Formation shallows upward in the southeastern MIG, where it is conformably overlain by the mixed carbonate-siliciclastic Iqqittuq Formation (Turner, 2009) which contains sulphate-facies evaporite beds (Jackson and Cumming, 1981; Kah et al., 2001). The Iqqittuq Formation is a northwest-deepening ramp that passes laterally to time-equivalent deep-water shale of the upper Arctic Bay Formation west of Tremblay Sound (Figs. 1, 2A). In the northwestern MIG, Arctic Bay Formation sandstone, siltstone and grey shale deepens upward into black shale that is locally laterally equivalent to large, deep-water carbonate mounds (Ikpiarjuk Formation) that accumulated in the vicinity of intragraben faults (Figs. 1, 2A,B,C). The upper Arctic Bay Formation black shale is, therefore, geometrically and temporally equivalent to both the Iqqittuq Formation and at least part of the Ikpiarjuk Formation (Fig. 2A). In the northwestern MIG, the Arctic Bay Formation is recessive and poorly exposed, with the exception of several locations where relatively continuous exposure is present in steep gullies and canyons. This formation has received no formal study since the work of Jackson and Iannelli (1981).

The Iqqittuq Formation carbonate ramp of the southeastern MIG is gradationally overlain by cyclic, peritidal facies of the Angmaat Formation (rimmed platform). This thick platformal unit passes westward over a short distance near Tremblay Sound to deep-water carbonate laminite of the Nanisivik Formation, which hosts most of the Zn-Pb showings in the MIG (Turner, 2009, 2011). The Nanisivik and Angmaat formations are separated from the overlying Victor Bay Formation by a pronounced subaerial unconformity (Turner, 2009, 2011). The Victor Bay Formation represents rapid marine inundation of this irregular landscape and development of a southwest-deepening mixed carbonate ramp. The Victor Bay basin was then tilted to produce uplift in the west and drowning in the east, recording basin inversion during poorly understood contractional deformation (Sherman et al., 2002). The upper Bylot Supergroup consists predominantly of terrigenous clastic deposits of the Nunatsiaq Group, which has been interpreted to represent an influx of sediment onto a complex topography associated with uplift to the distant west of the basin (Knight and Jackson 1994; Sherman et al., 2002).

In summary, the tectonostratigraphic history of the Bylot Supergroup is complex, and includes subtle regional subsidence during deposition of the Nauyat and Adams Sound formations, enhanced subsidence that formed grabens and controlled facies distribution during deposition of the Arctic Bay, Iqqittuq, Angmaat, Ikpiarjuk and Nanisivik formations, and pronounced differential uplift both after deposition of the Angmaat and Nanisivik formations, and again after deposition of the Victor Bay Formation. The Nunatsiaq Group (Knight and Jackson, 1994) is of uncertain tectonostratigraphic affinity.

Mafic dykes of the Franklin swarm (ca. 723-713 Ma; Heaman et al., 1992; Pehrsson and Buchan, 1999; Denyszyn et al., 2009) intruded along pre-existing graben-related fracture systems in the Neoproterozoic (Figs. 1,2A). Most gabbro-hosting structures show little to no evidence of fault displacement; they were deep-seated regional fracture systems inherited from the early graben, and experienced episodic reactivation and fracture propagation into overlying units.

Proterozoic rocks are unconformably overlain by undeformed Paleozoic carbonate and terrigenous clastic strata.

3. METHODS

Three stratigraphic sections, each hundreds of metres thick, were measured and described in detail in the deeper-water, western area of the upper Arctic Bay Formation. At all three locations, strata dip gently (6° to 18° northeast) and are well exposed in steep valley-walls. Valley-side exposures were examined for evidence of features that record evidence of syndepositional tectonic activity. Two of the sections were measured through the upper part of the formation at Shale Valley, east of the end of Adams Sound (Figs. 2B,C and 3A,C; SVC and SVE; 5 km apart). Samples of all rock types present were collected for laboratory analysis using a rock hammer and pocket knife after excavation of the material to a depth of ~10-30 cm. The area was glacially eroded and exposed only ~8,000 years ago, so deep weathering profiles are not present, but the material is inevitably to some extent weathered. A third section through the entire Arctic Bay Formation was measured on the north side of the Alpha River valley, 10 km west of Tremblay Sound and 90 km southeast of Shale Valley (Fig. 3B), but no true black shale is exposed there (although a thick covered interval may contain black shale).

Rock samples from Shale Valley Central (SVC), were analysed for their major and trace element compositions. Field samples were split into aliquots and dried at 70°C for 48 h to eliminate moisture. Each ~10 g sample split was hand-milled in an agate mortar to a fine powder. From this, a split was taken to perform a sequential 4-step loss-on-ignition (LOI) analysis on a single aliquot. Volatiles were driven off at 105°C in pure N_2 to quantify any remaining moisture, and then 3 steps of ignition under pure O_2 were undertaken, to successively burn off sulphides (up to 371°C), reduced carbon (up to 500°C) and carbonate and structural OH (up to 1000°C). A separate split was used to analyse hydrocarbon maturity and TOC by RockEval pyrolysis (Geological Survey of Canada – Calgary). A further split was taken to determine major elements by XRF (GeoLabs, MNDM), including total LOI. Finally, a 100 mg split was taken for trace element analysis at Laurentian University. Samples were digested by HF-HNO_3 at 170°C in Teflon beakers on a hotplate for 72 hours. This method does not completely digest zircon (e.g., Marx and Kamber, 2010) but has no adverse effect on transition metal concentrations, which are the main focus of the present investigation. Due to the high reduced C content of the samples, the fluoride residue that was obtained after digestion was twice attacked with 3mL of concentrated HCl to help break down unwanted organo-metallic complexes, which might otherwise compromise the metal yield. The chlorides were then twice converted with concentrated HNO_3 in preparation for dilution. The method was verified by analysis of the USGS shale standard SCo-1, a silty calcareous marine shale. Data for this standard obtained at Laurentian University are reported in Marx and Kamber (2010) and were found to be in good agreement with published values. The solutions were analysed by ICP-MS using the method outlined in Kamber (2009).

Whole-rock Pb-isotope data were obtained for the 19 lowermost samples in the SVC stratigraphic column. Lead was purified from the remaining stock solution of the trace element digest according to the method of Kamber and Gladu (2009) and analysed with the method described in Ulrich et al. (2010).

4. LITHOSTRATIGRAPHY

4.1 Shale Valley

Good exposures of the upper part of the Arctic Bay Formation are present on the northeast side of Shale Valley. An unknown thickness of lower Arctic Bay Formation strata separates these exposures from the underlying Adams Sound Formation. Intraformational truncation surfaces (ITS) that record subtle slope failure healed by deposition of new sediment over a low-angle fault scar are conspicuous on the hillsides and canyon walls of Shale Valley (Fig. 3C); strata trace laterally to non-equivalent units, and changes in structural orientation are evident across subtle contacts. Although no major intra-graben structural feature has been mapped in the valley, it is probable that a major northwest-trending intra-graben fault is present at or near Shale Valley (Fig. 1), based on the presence of ITSs and mound-related facies of the Ikpiarjuk Formation,.

4.1.1 Shale Valley Central (SVC)

At SVC, the lowest exposed strata of the Arctic Bay Formation (unit 1; 31 m thick) consist of shale-sandstone cycles 3 to 11 m thick, with hummocky cross-stratification (HCS) and gutter casts (Fig. 2B,C). A blue-white, iridescent weathering sheen is present on some centimetre-scale layers. Discontinuous rusty patches are rare. Medium-brown-weathering nodular lime mudstone is present at 31 m. From 31 to 60 m (unit 2; 29 m thick), the succession is dominated by dark grey shale with very minor sandstone interlayers. Medium-brown-weathering nodular lime mudstone is present at 44 metres, and a carbonate intraclast debrite at 42 m. Black shale (unit 3; 176 m thick), some of it slightly calcareous, is non-cyclic from 60 to 88 m. From 88 to 236 m, subtle shale-siltstone cycles, from 1 to 31 m thick, are marked by thin (generally <1 m), slightly more resistant and slightly paler caps. Conspicuous, 60 cm thick, buff-weathering carbonate layers with no distinctive structures are present at 122 and 136 m; a less pronounced carbonate layer is present at 87 m. Rusty-weathering shale is conspicuous between 62 and 74 m. Unit 4 (43 m thick) consists of argillaceous carbonate and black shale. From 236 m to 260 m, the lime mudstone is platy, resistant, and medium-grey-weathering, but from 260 to 279 m, lime mudstone is black and recessive. At 256 m, a 2 metre-thick, lenticular slump fold and debrite are present: contorted rafts of thin-bedded carbonate are entrained in the laterally discontinuous mass, as are volumes of dolostone intraclast floatstone (debrite). Approximately 30-40 m of cliff-forming, buff-weathering dolostone of the Ikpiarjuk Formation (unit 5) abruptly but conformably overlie black shale at 279 m. The dolostone consists of matrix- to clast-supported, chaotically disposed intraclasts: pale, equant dolostone clasts (Ikpiarjuk Formation) and tabular, medium brown intraclasts (Nanisivik Formation; here geometrically equivalent to upper Ikpiarjuk Fm.).

4.1.2 Shale Valley East (SVE)

At SVE, the lowest unit (unit 1; 96 m thick) consists of shale-sandstone cycles with hummocky cross-stratification, ripple cross-lamination and gutter casts; cycles are 3 to 24 m thick (Fig. 2B,C). A one m-thick, medium-brown-weathering nodular lime mudstone layer is present at 96 m. A blue-white, iridescent weathering sheen is locally present between 58 and 97 m. From 97 to 146 m (unit 2; 49 m), strata consist of dark-grey-weathering shale with scattered thin layers or lenses that have a blueish weathering sheen. A second nodular limestone 40 cm thick is present at 136 m. This unit is capped by a 1 metre-thick layer of cone-in-cone calcite. Black shale (unit 3; 67 m) dominates the section from 147 to 214 m. Subtle shale – siltstone cycles like those at Shale Valley Central are 2 to 18 m thick. Scree material indicates that similar strata underlie a covered interval from 214 to 237 m. Although most of the interval from 237 to 277 m (unit 4; 40 m) is covered, scree composition indicates that its composition is similar to that of the interval between 277 and 303 m: black shale intervals (1-7 m thick) alternate with more resistant, one m-thick bands consisting of clusters of layer-parallel, laminar concretions approximately 1 mm thick and up to decimetres wide; these platy, discoidal, intrastratal concretions consist of dark, coarse calcite crystals radiating unevenly from a central area. Rarely, this concretionary material is present as concretion clasts in debrites, indicating that they formed early in the shallow subsurface. Unit 5 is an in situ line of frost-heaved rubble of a 50 centimetre-thick layer of tabular carbonate intraclast debrite belonging to the distal margin of an Ikpiarjuk Formation mound. Unit 6 consists of shale scree ~1.5 m thick. Overlying, medium-brown-weathering, homogeneous, medium-crystalline dolostone with a strong but ephemeral bituminous odour when freshly broken belongs to the basal Nanisivik Formation (unit 7; in situ frost-heaved rubble).

4.2 Alpha River

Strata of the Arctic Bay Formation are well exposed in canyons on the north side of the Alpha River (Fig. 3B). The top of the Adams Sound Formation is present, although generally covered, at the level of the river. Exposure ends at a plateau approximately 550 m higher, roughly where Arctic Bay Formation shale passes to a complex array of overlying dolostone facies of the Iqqittuq, Angmaat, Nanisivik and Ikpiarjuk formations (Figs. 2B, 3B).

The contact with the underlying Adams Sound Formation is not exposed, and a covered interval between its inferred position and the lowest strata exposed is estimated to be 40-60 m thick. Lithostratigraphic unit 1 consists of siltstone – sandstone cycles and is 332 m thick. In the lowest Arctic Bay Formation strata (0-33 m), quartz arenite units 3-4 m thick are separated by covered intervals. Overlying strata (33 m to 332 m) consist of shale-sandstone cycles. Cycles are conspicuous from their weathering profiles, are 5 to 25 m thick, and thicken upwards, with a decreasing sandstone component. Ripple cross-lamination, HCS and synaeresis cracks are common to approximately 200 m, above which level sedimentary structures become fewer and less distinct. Scattered cone-in-cone calcite concretions are present between 80 and 180 m. Unit 2 (181 m thick; 332 to 513 m) consists of shale-sandstone cycles that are 25 – 50 m thick. Thin (<1 m), laterally continuous, medium-brown-weathering nodular limestone layers are present at 332 m and 406 m, and scattered carbonate nodules are present at 405-425 m and 460-480 m. A resistant-weathering interval containing sandstone layers is conspicuous between 485 and 513 m and contains hummocky cross-stratification and clasts of cross-laminated sandstone in sandy debrites. The top of this interval contains one thin bed with polygonal cracks of unknown derivation, and mudstone clasts in graded beds. Shale throughout the exposed section is various shades of dark grey, and never truly black. It is commonly rusty-weathering near cycle bases between 80 and 210 m, and two very conspicuous rusty-weathering intervals are present at 405-415 m and 425-435 m; in both cases these rusty intervals are associated with nodular limestone. An iridescent blue-white weathering sheen is present on some centimetre-scale layers between 33 and 418 m, and is especially well-developed between 317 and 333 m.

An estimated 125 m (unit 3a) that is covered separates the lower and upper exposures of the Arctic Bay Formation. Shale-dominated strata of the upper Arctic Bay Formation (unit 3b; 148 m) are exposed on a slope between the first plateau above the Alpha River and the upper plateau (regional high point). West of the measured section, this shale exposure is stratigraphically equivalent to a level slightly below the base of a mound of the Ikpiarjuk Formation (Bellevue Mound; Turner 2009). Above the grey shale succession is dolostone exhibiting interlayered Nanisivik Formation and Angmaat Formation lithofacies. The grey shale interval is laterally equivalent to an exposure of distal Iqqittuq Formation several hundred metres to the east, which consists of interlayered shale, locally slump-folded ribbon to parted limestone (thin-bedded lime mudstone with shaly interbeds or partings) and intraclast debrites (Fig. 3B). Uppermost Iqqittuq Formation strata are affected by ITSs in nearby exposures (Fig. 3D). Iqqittuq strata are overlain by Angmaat Formation massive, pale, cherty dolostone. Given the geometric relations among these units, tens of metres of uppermost Arctic Bay Formation are covered between the uppermost exposed shale in the measured section and the mound-margin wedge, and that the distal Iqqittuq Formation is equivalent to the uppermost Arctic Bay Formation. Owing to scree cover, it was not possible to make an accurate geometric connection between interlayered shale and limestone of the Iqqittuq Formation and the upper part of the Arctic Bay Formation. Neither was it possible to sample the recessive, shaly interlayers of the outer Iqqittuq Formation.

The entire exposure above the covered interval (148 m; unit 3b) consists of dark-grey-weathering shale with very rare, 10 cm-thick orange-brown dolomudstone layers.

No stratigraphic section was measured between Shale Valley and lower Alpha River, but the Arctic Bay Formation has been examined immediately below its contact with the Nanisivik Formation at numerous locations across the central Borden Peninsula. Almost invariably, the uppermost Arctic Bay Formation in this region consists of black shale with intrastratal, millimetre-thick, discoidal black concretionary layers of coarse calcite crystals like those in the uppermost part of the SVE section.

5. GEOCHEMICAL RESULTS

5.1 Geochemical data

Analytical data for section SVC can be used to provide information about both sediment provenance, which can be used to test depositional models based on field and sedimentological data, and the chemical evolution of the water column below which the sediment accumulated.

The latter information is relevant to understanding Precambrian ocean-atmosphere evolution and SEDEX potential of the basin.

5.1.1 Rare earth element systematics

The samples selected for laboratory analysis comprise a variety of lithologies: conspicuous iridescent siltstone nodules, rusty sandstone, calcareous shale, black shale, rusty shale, carbonate nodules, carbonate laminite and a carbonate slump. Although from a sediment provenance perspective the siltstone nodules and carbonate rocks are of limited use, the upper continental crust (here Mud of Queensland (MUQ); Kamber et al., 2005) normalised rare earth element (REE) patterns of these lithologies are first briefly discussed (Fig. 4).

Two iridescent Mn-rich siltstone nodules (Table 1) have inverted V-shaped REE patterns (into which Y is inserted at its position of relative ionic radius). The two important aspects of these patterns (grey bars in Fig. 4A) are the absence of a Ce anomaly and the dip in Y compared to neighbouring Dy and Ho. These features indicate that the Mn-rich nodules are probably diagenetic in origin. For comparison, a representative REE pattern from a diagenetic Central Pacific modern deep-sea Mn nodule (Fig. 4A) is shown. Although it is flatter overall (probably due to different local lithology) it highlights the characteristic dip in Y and the lack of a Ce anomaly. In contrast, hydrogenous Mn concretions have positive Y anomalies and very strong positive Ce anomalies (e.g., Ohta et al., 1999). In a stratified ocean basin with a reduced lower water mass, such as probably existed in the Mesoproterozoic, excess Ce may have been released from Mn-oxyhydroxides, and the absence of a positive Ce anomaly, on its own, might not be sufficient to distinguish between hydrogenous and diagenetic nodules. The combination with the concentrations (1.05 and 4.33 wt%) of these two samples also support diagenetic uptake of the

REE by phosphates. However, the experimental data of Byrne et al. (1996) are at odds with empirical observations regarding the behaviours of Y and Ho.

Sample SVC-60, a carbonate nodule, is also Mn-rich (13,800 ppm), and its REE pattern has similarities with those of the siltstone nodules. The (weak) positive Ce anomaly of these three samples is positively correlated with the total REE content (r^2=0.810, not shown) and with the Co/(Cu+Ni) ratio (r^2=0.829, not shown). This pattern is similar to the systematics of modern Mn nodules (e.g., Fig. 5a of Ohta et al., 1999) and indicates that the siltstone nodules are diagenetic in origin, whereas the Mn-oxides in the carbonate nodule have a mixed hydrogenous and diagenetic origin.

Moving up in the stratigraphy, regardless of stratigraphic height and carbonate content, the remaining samples have similar patterns to upper continental crust, and appear flat when normalised to upper continental crust. In more detail, when compared to the normalising upper crustal composite, they show a 1.7-fold light over middle REE (LREE and MREE, respectively) enrichment and flat MREE to heavy REE (HREE) patterns. The average normalised La/Gd of all of the shales is 1.68±0.29, whereas the normalised Gd/Lu ratio is 1.17±0.21. This suggests that the sediment was derived from a source that was more chemically evolved than average upper continental crust.

The three non-nodular black shale samples richest in carbonate (SVC-71, 89 and 92) all have negatively sloped normalised REE patterns (Fig. 4B), variably negative Ce anomalies, and well-developed positive Y anomalies. These are features found in sediment that precipitated from oxygenated water (required to explain the negative Ce anomaly) that is restricted from the open ocean (explaining the negative overall slope; Kamber et al., 2004). Figure 4C shows the

REE pattern of the most calcareous shale (SVC-80), which shares the negative Ce anomaly and the positive Y anomaly of the carbonate-rich samples (shown for comparison). These anomalies are absent in shale samples that contain much less carbonate (shown as an example is SVC-86). Carbonate admixture thus introduces Y and Ce anomalies into otherwise smooth REE patterns.

The REE systematics of the black shale, rusty shale and rusty sandstone exhibit an interesting stratigraphic relationship (Fig. 5). There is a marked general decrease in overall REE abundance from the bottom to the top of the formation. The overall REE content is very strongly related to Al content (r^2 = 0.983), but only for samples with Al_2O_3 up to 11.5 wt%, indicating that REE systematics in these samples is related to argillaceous content. However, for samples with Al_2O_3 of >11.5 wt% (i.e., all of the shale samples), the correlation with total REE content breaks down completely (r^2 = 0.001). Hence, the REE systematics of the shales are not determined by the amount of clay.

The trend in REE content is accompanied by a change in REE pattern. The samples from units 1 and 2 have essentially identically shaped REE patterns, pointing to a common sediment source. The two lowermost analysed samples from unit 3 (66-84 m in Fig. 5) share the LREE and MREE characteristics with the lower units, but are much more depleted in the heavy REE (HREE), which signifies a change in sediment source. The trend continues in the samples representing stratigraphic height between 94 and 109 m. The overlying, major part of unit 3, represented by stratigraphic height from 132 to 231 m, have nearly constant REE patterns, indicating a constant sediment source. The uppermost samples from unit 4 are the least enriched in REE overall, which may indicate yet another slight change in sediment provenance.

5.1.2 Quantification of effect of carbonate and clay content on REE systematics

To test the qualitative finding that the REE patterns of the black shale were influenced by carbonate, major element and 4-step LOI data were obtained (Table 1). Comparison of TOC data with the LOI step from 375 to 500°C shows excellent correlation (although biased towards 15% higher values in the latter, possibly due to loss of organic S and/or N). It is reasonable to assume that combustion of carbonate occurs mainly between 500 and 1000°C under an O_2 atmosphere. Observed values for this LOI step were compared with theoretical, calculated estimates by attributing CaO and MgO to carbonate. When the entire Ca and Mg inventory is allocated to carbonate, this comparison (Fig. 6A) shows that the observed and calculated LOI values correlate very closely ($r^2 = 0.970$) with a slope of 0.96. This suggests that the original clay minerals were low in Ca and Mg and had experienced a significant degree of weathering. It also shows that even in the shale samples that have little Ca and Mg, a small amount of carbonate is present. Furthermore, the stoichiometric Ca:Mg ratio shows that in all of the shales, the carbonate is dolomite. Finally, the dolomitic composition is in strong contrast to that of the crystal concretions (sample 09-SVC-89), which are pure Ca-carbonate. The strong influence of the admixed dolomite on the REE pattern can be quantified when plotting (CaO+MgO) vs. the Y/Ho ratio (Fig. 6B). The calcareous shale samples with high LOI have higher, super-chondritic Y/Ho. Importantly, the calcite crystal concretion plots off the strong trend ($r^2 = 0.886$) defined by the shales, which is caused by admixture of dolomite rather than of calcite.

In fine-grained siliciclastic sediment, clay content is commonly the dominant control over the total lanthanide concentration (∑REE). In the studied samples, however, Al_2O_3 controls REE content only in the samples with low clay content (Fig. 6C). In the more clay-rich shales, the correlation breaks down, suggesting that the REE content of the clay was variable, and as shown in Figure 5, changed systematically with stratigraphic height. This is strong evidence for multiple sources of clay-rich sediment.

The Al_2O_3 content of shale samples is strongly inversely correlated (r^2 = 0.906) with (MgO+CaO), and so the combined evidence suggests that the shale is a mixture of two sedimentary components: organic-C-rich clay, and dolomite. In those samples poorest in clay, total lanthanide concentration is lowest, and therefore the marine REE characteristics are best expressed (i.e., highest Y/Ho and most negative Ce anomaly).

5.1.3 Conservative elements

Ratios of conservatively behaving high-field-strength elements such as Zr/Hf, Nb/Ta, Nb/Th show little change through the entire stratigraphic section. For example, there is only a slight decrease in Nb/Ta with increase in stratigraphic height. The lowermost two samples (from units 1 and 2) have average Nb/Ta of 15.03±0.73, followed by the unit 3 samples (n=13) averaging 14.35±0.42, which are capped by unit 4 samples with an average of 14.03±0.14.

A general decrease in conservative, incompatible trace element concentration with time, which is evident from the position of the REE patterns (Fig. 5), is conspicuous in plots of concentration vs. stratigraphic height (Fig. 7A). Most of the commonly used immobile trace elements, such as Ti, Zr, Nb, Hf, Ta, Th and the REE, as well as less commonly studied elements such as W and Be, show marked decreases in concentration, on the order of 3- to 5-fold, from bottom to top (Fig. 7A). This trend is not present in the compatible elements (e.g., Cr, Sc), the most lithophile elements (e.g., Li, Cs), or in Al_2O_3. There is no correlation between high-field-strength element content and Al_2O_3, indicating that clay minerals did not control supply of these elements. Instead, the trend in high-field-strength element concentration (Fig. 7A) is likely caused by a gradual decline of heavy mineral content. In the samples above the iridescent Mn-rich siltstone nodules, the content of Ti, which is commonly used as a proxy for the heavy minerals titanite, ilmenite and rutile, correlates positively with Th (r^2 = 0.808), Zr (r^2 = 0.933), Nb (r^2 = 0.913) and Sn (r^2 = 0.873), suggesting that zircon and cassiterite were also important detrital components.

5.1.4 Metal chemostratigraphy

The most interesting geochemical feature from both basin evolution and SEDEX potential perspectives is that the general decline in incompatible conservative element concentrations with stratigraphic height is not at all mirrored by many transition metals and redox-sensitive elements. Instead, many of these metals show the opposite stratigraphic evolution, becoming more enriched with increasing stratigraphic height, and reaching peak values at ~200 m (Fig. 7B). The strongest variation in concentration is found for the elements Mo (240x), Ag (33x), Cd (20x) and V (7.6x); Ni, Cu, Zn and U also show considerable concentration increases that contrast with the decreasing trend of the high-field-strength elements. The concentration increase is not monotonic with stratigraphic height, but shows a systematic pattern with maxima between 145 and 200 m (Fig. 7B). Because the Nb/Ta and REE systematics of the studied shales are different from average upper continental crust, it is not feasible to calculate conventional enrichment factors. Instead, the detrital contribution to the shale's metal inventory was removed by using metal ratios relative to conservative elements. The resulting stratigraphic enrichment trends are smoother (Fig. 7C) and the overall concentration contrast increases. For example, although the V concentration alone varies by a factor of 7.6, the V/Nb ratio changes by a factor of 25.3. Similarly, Cd, whose elemental concentration range is 20, expresses a relative enrichment range (calculated as Cd/Th) of 77. The relative enrichment of

V and Cd peaks at 200 m (Fig. 7C), whereas Mo, U, Ni, Zn and Cu show two maxima, at ~145 m and ~200 m.

As is anticipated from the coherent behaviour in the context of stratigraphy, the metal/conservative element ratios are strongly correlated. For example, V/Nb correlates with Cd/Th (r^2=0.846) and Mo/Hf (r^2=868; Fig. 8A), which itself correlates, although not as strongly, with U/Th (r^2 = 0.339), which in turn correlates with Ni/Cr (r^2=535; Fig. 6B). The possible origin of these trends is discussed below.

<u>5.1.5 Pb-isotope systematics</u>

The whole-rock Pb-isotope data form a co-linear array in common Pb space (Fig. 9). When the two most deviating samples (SVC-71 and 75) are omitted, the remaining 17 data points define an isochron (MSWD = 1.6) of 1137±98 Ma. Furthermore, 17 of the 19 data points (excluding SVC-72 and 80) also yield an $^{238}U/^{206}Pb$ errorchron of 1067±100 Ma, and 14 samples (excluding SVC-51, 58, 72, 79 and 80) define an $^{232}Th/^{208}Pb$ errorchron of 1059±120. These are three independent age constraints yielding a weighted mean of 1092±59 Ma. This date, although not very precise, is interpreted as the age of deposition and is in agreement with other chronological constraints. In terms of original Pb-isotope composition of the sediment, the isochron projects between the coeval mantle evolution composition and that of juvenile upper continental crust. This suggests a mixed sediment supply dominated by juvenile sources, which is in agreement with the high Nb/Ta ratio, other provenance indicators, and the local geology.

6. INTERPRETATON

6.1 Basin Evolution and Provenance Information

The evolution of the northwestern MIG during deposition of the Arctic Bay Formation can be reconstructed using lithostratigraphic profiles from Shale Valley and Alpha River (Fig. 10) together with regional stratigraphy (Turner, 2009). A rift-like phase of the MIG initially developed when geographically limited excessive subsidence formed a west-deepening ramp (Arctic Bay Formation) flanked at its southern and northern margins by coarse terrigenous detritus (Fabricius Fiord Formation; Jackson and Iannelli, 1981; Scott and deKemp, 1998) that was deposited along the flanks of horsts veneered with Adams Sound Formation quartz arenite and Nauyat Formation basalt. The northwestern, lower Arctic Bay Formation was initially characterised by very gentle northwest-ward deepening in a regionally storm-dominated, strongly cyclic, sandy to muddy setting. Waning of terrigenous input produced a protracted upward-fining succession that was punctuated by deposition of rare benthic carbonate mudstone, and eventually led to black shale deposition in the outer, northwestern parts of the muddy ramp. In the southeastern MIG, carbonate deposition of the Iqqittuq Formation, laterally equivalent to the black shale interval in the northwest, was punctuated by intervals of bedded sulphate-facies evaporite.

Direct evidence of synsedimentary faulting during black shale deposition is present in the form of ITSs, which represent areas where deep-water slopes failed and the resulting surfaces, cutting at low angles across underlying strata, were overlain by new sediment layers parallel to scar surfaces. Such ITSs and the associated evidence for locally variable sediment composition and accumulation rates are present both at Shale Valley (lower and upper Arctic Bay Formation) and at Alpha River (distal Iqqittuq Formation, which is laterally equivalent to upper Arctic Bay Formation black shale). Given the very subtle slope gradient from the central part of the MIG to the northwestern part (at most several tens of metres of topographic differential, across a lateral distance of ~100 km), this type of over-steepening and gravitational failure of slopes cannot have been caused by normal sedimentary or subsidence processes, and was instead probably a product of tectonic adjustment along major intra-graben faults. The ITSs documented to date are in the immediate vicinity of such faults. In some cases the failure direction was at a high angle to or even opposed to the regional northwest-deepening gradient of the basin floor, supporting the interpretation that the ITSs were caused by local over-steepening associated with intermittently active fault systems.

At Shale Valley, an ITS that affected SVE but not SVC removed part of the black shale of unit 3. Consequently, unit 3 black shale is markedly thinner at SVE than at SVC, owing in part to removal of at least several tens of metres of section at a conspicuous ITS. Unit 4 is strikingly different in the two Shale Valley sections: the SVC location received resedimented, slumped carbonates, inferred to be related to a mound- and fault-related slope, whereas the SVE location accumulated black shale in which concretionary calcite grew in the shallow subsurface. Pronounced differences in the thicknesses of these geometrically (but not temporally or paleoenvironmentally) equivalent units are supported by geochemical evidence (described below).

Indirect evidence of subtle syndepositional faulting is provided by large, elongate, deep-water (sub-photic zone) carbonate mounds of the Iqqittuq Formation, which grew during deposition of the upper Arctic Bay Formation black shale, only in the vicinity of major intra-graben faults (Turner, 2009). It is inferred that fissures related to the faults reached the sea-floor and dilated in response to subtle tectonism to serve as conduits for fluids associated with mound development.

Shale deposition ended abruptly owing to tectonic adjustment that produced a semi-restricted, terrigenous-sediment-free basin differentiated by a tectonic barrier into two zones. In the northwestern zone, carbonate precipitated either in the water column or directly on the sea floor, and accumulated as monotonous, millimetrically laminated deep-water dolostone, (Nanisivik Formation). The southeastern zone was characterised by cyclic accumulation of lagoonal to peritidal carbonate rocks with abundant sea-floor carbonate dendrites and "abiogenic" stromatolites, which are widely recognised as indicators of evaporative carbonate oversaturation (Angmaat Formation; Turner, 2009).

Prior to development of the graben, the paleoclimate had been humid enough for the existence of river systems that supplied quartzose sediment to the predominantly marine Adams Sound Formation. By the time that the prograding, carbonate-dominated Iqqittuq Formation was accumulating in the southeastern MIG (laterally equivalent to black shale of the upper Arctic Bay Formation), the climate had become arid enough to result in deposition of bedded sulphate-facies evaporites (Jackson and Cumming, 1981; Kah et al., 2001). Still later, the climate became humid once again, as indicated by karstification of the upper Victor Bay Formation (Sherman et al., 2002).

The inferred low Ca and Mg content of the clay in the analysed shale supports a strongly weathered sediment source. In terms of provenance, the shale has several notable features that agree with respect to sediment provenance. The high Nb/Ta (14-15) of the sediment is much higher than typical continental crust (~11.5; Kamber et al., 2005) and is a strong indication that the sediment source was dominated by basalt (with Nb/Ta>15) with a only a subordinate felsic component. This finding is supported by the REE patterns of the shales, which show greater LREE than MREE and only mild MREE over HREE enrichment. Such kinked REE patterns (e.g., Xu et al., 2005) as well as unusually high Nb/Ta (Murphy et al., 2003) are characteristic of alkali basalts associated with continental rift magmatism.

6.2 Origin of metal enrichment

The geochemical data (Figs. 7B,C, 8) document consistent enrichment of a number of metals in the black shale part of the SV sections, chiefly in unit 3. In order to assess the extent to which this enrichment could be relevant to the SEDEX potential of the basin, it is necessary to determine the cause of metal enrichment. The first-order question is to determine whether the metal enrichment occurred during sediment settling (by scavenging from the water column or along the water/sediment interface) or during diagenesis.

The most widely discussed mechanism (e.g., Lyons et al., 2009) for redox-sensitive metal enrichment in black shale involves a chemically stratified water column and a particle shuttle (organic, metal oxyhydroxides, or sediment) that acts as a direct carrier of metals or helps to maintain physico-chemical conditions that are conducive to metal incorporation into the sediment (e.g., euxinia above or within the sediment). The presence of anoxic bottom-water conditions during deposition of black shale of SVC units 3-4 is not in question. The TOC, as determined by RockEval pyrolysis as well as the third step of LOI (375 to 500°C), which is dominated by reduced C, averages between 5 and 6 wt%, suggesting that high primary productivity in the upper part of the water column may have helped to maintain anoxic and, at times, euxinic conditions at depth, in a rift basin that may have been restricted and may have had a primary chemocline typical of the Mesoproterozoic ocean as a whole (e.g., Canfield et al., 2008). Most samples have high Fe/Al ratios (on average 0.71, but up to 2.1) that are very similar to other Precambrian shale deposits (e.g., Raiswell et al., 2011). Although no Fe-speciation and quantitative S data were obtained, the combination of high TOC, high Fe/Al and S contents, and qualitative Fe/S ratios similar to pyrite stoichiometry, strongly suggests that euxinic conditions were reached at times during deposition of the shales of unit 3.

The negative Ce anomalies in limestone beds and nodules argue for an uppermost water column that was sufficiently oxygenated to convert Ce^{3+} to Ce^{4+}. Conversely, the Mn- and phosphate-rich samples have slight positive Ce anomalies, suggesting that at depth, below the chemocline, Ce may have been reduced back to Ce^{3+}. Furthermore, the limestone nodules have positive Y/Ho, whereas the phosphate-rich Mn nondules have subchondritic Y/Ho. These systematics afford an opportunity to propose an origin for the dolomite, which may have precipitated from the uppermost, oxygenated water column and rained down as particles, or may have formed within the sediment due to alkalinity changes driven by sulphate-reducing bacteria [i.e., the “organogenic dolomite” described by Mazzullo (2000)]. The REE systematics argue in favour of a upper-water-column origin for the carbonate in the black shales, but allow for the possibility of diagenetic conversion of limestone to dolomite, because this process does not necessarily change REE patterns (e.g., Webb et al., 2009). Combined C- and O-isotope evidence would be needed to further elucidate the origin of dolomite.

Despite these coherent observations in favour of a redox-stratified basin with anoxic bottom waters, there is no straightforward correlation between TOC, Fe/Al ratio, Mn, and qualitative S content.

None of the samples other than the Mn-rich nodules, contains an appreciable positive Ce anomaly (Figs. 4 and 5). In a redox-stratified basin, Ce is either oxidised in the shallow water column, or once trivalent Ce is adsorbed onto the hydroxide ion (Bau and Koschinsky, 2009), and is then transported with particles into the anoxic, deeper water, where it is released. For this reason, both Fe and Mn-hydroxides are very strongly enriched in Ce relative to neighbouring La and Pr, giving rise to very characteristic REE patterns with strong positive Ce anomalies (e.g., Ohta et al., 1999). Such an anomaly is not present in SVC shale. Manganese oxides also have sub-chondritic Y/Ho ratios, another feature that is absent in the shale. From the combined evidence, it can be concluded that the total authigenic metal budget in the sediment has multiple origins that include clastic sedimentation rate, reduced C supply, Mn- or Fe-oxyhydroxide shuttles, availability of HS^-, and other factors, none of which exerted dominant control. The lack of correlation among these chemical proxies is not unique to the black shale studied here (e.g., Raiswell et al., 2011), and does not automatically imply post-depositional modification (e.g., Cruse and Lyons, 2004).

Molybdenum enrichment reaches concentrations of 50 ppm (Fig. 7C; the highest reported values for Mesoproterozoic black shales; see Scott et al., 2008) and offers an opportunity to explore possible reasons for overall metal enrichment. Elevated Mo concentrations generally result when Mo that is complexed with organic C encounters elevated concentrations of HS^- either in the water column or in sediment pore waters, at which stage it is scavenged effectively as thiomolybdate (e.g., Algeo and Tribovillard, 2009). In the Arctic Bay Formation, despite the very strong Mo-enrichment in many of the studied samples, there is no discernible correlation of Mo/Hf with Fe/Al (r^2= 0.207), estimated reduced C content ($LOI_{375\text{-}500}$; r^2 = 0.004) or qualitative S content (r^2 = 0.017). Lack of correlation persists regardless of whether clastic input is corrected for with Al, Ti or as enrichment factors. Instead, there is a significant positive correlation with the Y/Ho ratio (r^2 = 0.650) and with the carbonate (dolomite) content ($LOI_{500\text{-}1000}$; r^2 = 0.659). In view of the strong correlation of Mo enrichment with other metals such as V (Fig. 8A,B), it is not surprising that V/Nb is also strongly correlated with Y/Ho ($r^2 = 0.815$, Fig. 8C). Dolomite content of the black shale correlates with metal enrichment and so the most parsimonious explanation for metal enrichment in the shale is the activity of a dolomite (or dolomite precursor) particle shuttle or a dolomite metal trap in the sediment. No attempt was made to analyse the fine-grained carbonate separately for metal content.

One observation from the present dataset, however, indicates that the stratigraphic metal distribution as measured today may not be completely primary. Authigenic metal enrichment should be strongly associated with elevated Co concentrations. For example, hydrogenous FeMn-oxide crusts have very elevated Co/(Ni+Cu) (e.g., Calvert and Price, 1977). However, the SVC black shale data show no correlation whatsoever between Co/(Ni+Cu) and Mo, V, C or U enrichment. Other studies have previously documented complex redox-sensitive authigenic metal distributions in black shale (e.g., Pennsylvanian black shale from Oklahoma in Cruse and Lyons, 2004). In actively rifting basins that experience low-T hydrothermal discharge, additional metal sources other than a stratified water column may significantly increase metal content (as proposed for Devonian black shale in Yukon; Hulbert et al., 1992), which might lead to the dissociation of Co vs. (V,Mo, U) trends.

An alternative working hypothesis is that the metal distribution, as it is found today, was affected by secondary basinal fluids (e.g., Leventhal, 1991). In this model, the overall enrichment of redox-sensitive metals in the entire sediment body was originally caused by metal transfer into the sediment in a stratified water body with anoxic and at times euxinic bottom waters (as discussed above). Although the stratigraphic relative metal enrichment appears at first glance (e.g., Fig. 7) to be systematic, there is a conspicuous lack of correlation between metal enrichment and Fe/Al, Mn, or TOC content. Instead, the metal enrichment appears to track the dolomite content of the shales. If the dolomite formed in situ due to increased alkalinity caused by sulphate-reducing bacteria, for example, it is possible that the metals were enriched locally from pore waters. Alternatively, if the dolomite represents a primary sediment component, it could be hypothesised that when diagenetic fluids migrated through the sediment column upon compaction, the carbonate in the calcareous shales would have acted as a redox trap, elevating the fluid's pH, affecting metal solubility, and causing precipitation.

Regardless of the exact mechanisms that caused metal enrichment, an important observation from this study is that absolute concentrations of redox-sensitive metals in black shales (e.g., Mo) must be used with caution to infer ancient ocean conditions, particularly when elevated metal contents are associated with subtle carbonate-bearing horizons.

6.3 SEDEX potential of the black shale basin

Depositional settings that are associated with SEDEX/CD potential commonly exhibit evidence of synsedimentary extensional faulting under euxinic deep water, starvation of terrigenous and precipitated sediment, and topographic compartmentalisation of the basin floor into small-scale sub-basins whose bottom-water chemistry could evolve independently of other parts of the basin (Leach et al., 2005; Goodfellow, 2007; Goodfellow and Lydon, 2007; Leach et al., 2010). Also favourable is the presence of evaporites in strata that are laterally and temporally related to the black shale interval, which create dense brines that sink and acquire metals as they migrate through buried aquifer units (e.g., Russell et al., 1981; Goodfellow et al., 1993; Leach et al., 2005). Virtually all of the structural and stratigraphic preconditions for SEDEX/CD deposition are amply evident in the Arctic Bay Formation. These positive attributes are then greatly reinforced by the basin's geochemical history.

Geochemical evidence depicts a lengthy time during which the deep-water area of the upper Arctic Bay Formation was occupied by stratified water with reducing or euxinic bottom water. The water column in the basin was therefore capable of converting metals supplied as solutes into a particulate component of the sea-floor sediment. Of the base metals present in anomalous concentrations throughout the black shale interval, Zn covaries with Mo, suggesting that, like Mo, it was removed from solution by reduction. Unlike Mo, however, Zn, and to a lesser extent Ni, were probably not sourced from terrestrial weathering, and so if the enrichment in Zn and Ni are primary, these metals would have have been supplied by vented fluids. Both the carbonate rocks and the black shale lack positive Eu anomalies, which is evidence against high-T (i.e., >250°C) hydrothermal-vent-type fluids (e.g., Kamber, 2010) and suggests that the fluids were probably of the off-ridge-axis, diffuse, low-T variety. Zinc and Ni could have been supplied from leaching of the underlying pile of fine terrigenous sediment by basinal brines. This is a plausible source for the Zn, and commonly inferred in SEDEX systems (e.g., Russell et al., 1981; Goodfellow et al., 1993). The stratigraphic spacing of samples analysed in this study was coarse, and intervals with elevated metal concentrations could easily have been missed. Although Zn concentrations do not reach economically meaningful concentrations at the stratigraphic levels tested in this study at this particular location, the broad stratigraphic, structural and geochemical conditions for a SEDEX system were present.

Mineralising systems other than SEDEX-type should be considered for the black shale succession. Molybdenum and other redox-sensitive elements were stripped from sea water during black shale deposition, and it could have been possible, with a very low sedimentation rate of fine terrigenous material, for Mo, U, and other redox-sensitive metals to reach high concentrations on the sea-floor. There is no evidence of such elevated concentrations in the stratigraphic levels tested at the one location addressed by this study, but the sample spacing was coarse, such that geochemically interesting intervals may have been overlooked by this survey. The sedimentary and geochemical evolution of other black shale sub-basins of the Arctic Bay Formation may have been more favourable for deposition of redox-sensitive metals.

Unit 1 (0-31 m) of the succession at SVC contains siltstone nodules to layers that are conspicuous in outcrop from their iridescent, violet-white weathering sheen. These units are characterised by elevated concentrations of Mn, Pb, As, Ni, Zn and Fe, a composition that resembles that of modern deep-sea Mn nodules. If this composition was primary, the abundance of Mn in these layers reflects deposition below a chemocline, but one characterised by a geochemical composition that is markedly different from that of the later black shale basin, as reflected by REE composition.

6.4 Depositional age

In the eastern MIG, the Arctic Bay Formation is overlain by carbonate-dominated strata of the Iqqittuq and Angmaat Formations (collectively formerly known as the Society Cliffs Formation), the Victor Bay Formation, and the Athole Point Formation. This carbonate-dominated succession shows a distinctive $\delta^{13}C$ curve that has been correlated with carbonate strata in Mauritania (Kah et al., 1999) and dated at 1105±12 to 1109±37 Ma (Re-Os; Rooney et al, 2010). The identical (within its larger error) U-Th-Pb shale depositional age of 1092±59 Ma yielded by the present study for black shale that is temporally equivalent to part of the carbonate-dominated succession (i.e., equivalent to upper Iqqittuq Fm.) fits well with this chronology. The succession may be significantly younger than a previous estimate of approximately 1199 ± 24 Ma (Kah, unpublished data, in Kah et al. 2001).

7. DISCUSSION

7.1. Dynamics of dissolved molybdenum in the Mesoproterozoic ocean

Black shale geochemistry is rapidly becoming a major source of information used to infer planetary atmospheric evolution and ocean ventilation (e.g., Scott et al., 2008; Dahl et al., 2011). The present study provides a large new dataset that can be used to qualify some of the inferences made from global compilations.

The REE patterns of the Arctic Bay Formation calcareous black shale suggest carbonate (dolomite or dolomite precursor) formation in oxygenated water. Given the high TOC and reduced metal content of the shales, this provides strong evidence for a rift basin in which a chemocline had developed. It also supports a globally oxidizing atmosphere. However, the observation of anoxia in a rift basin does not imply that the global deep ocean was anoxic.

A major argument in favour of an anoxic and sulphidic post-1.8 Ga Proterozoic deep ocean is the relatively low Mo content of black shale, in comparison with Paleozoic equivalents (Scott et al., 2008). The reasoning behind this argument is that the marine inventory of Mo in a sulphidic ocean could never have increased greatly because of the continuous drawdown of Mo into pyrite across the entire ocean floor. The maximum Mo concentrations encountered in this study (~50 ppm) agree with global compilations (e.g., Scott et al., 2008), but the present dataset is from a localised rift graben basin, rather than a setting fully linked to the global ocean. If the basin water was not in full exchange with the open ocean, the relatively limited Mo enrichment encountered in the black shale can only be used to infer that the Mo concentration in this restricted basin never reached the levels of the Phanerozoic ocean. This observation does not preclude the possibility that open seawater had a much higher Mo concentration.

Because the primary source of Mo to the ocean is generally assumed to be fluvial, the number and distribution of rift basins themselves may also be relevant. Molybdenum supplied by rivers to rift basins would be removed effectively on account of the likely anoxic/euxinic nature of these basins. Hence, at times of supercontinent rifting, the global ocean Mo inventory may be substantially lower than during times of dispersed continents because of the combined effects of reduced fluvial flux and enhanced scavenging of metal into anoxic/euxinic rift basins.

Regardless of the issue of local water versus open seawater chemistry, a further complication arises from the present study: the possibility of secondary enrichment of redox-sensitive metals, such as Mo, into thin stratigraphic horizons. Geochemical studies generally assume that Mo content is a reflection of primary sediment chemistry and that Mo is hosted by pyrite (e.g., Lyons et al., 2009). At Shale Valley Central, however, high Mo content is associated with high dolomite content and may not be a true reflection of the basin's water chemistry. This may not be a unique situation. For example, the proposal of a brief Neoarchean global oxidation event was based in part, on elevated Mo contents in the McRae shale (Hamersley Basin, Australia; Anbar et al., 2007). The enriched interval in the 30 m-thick S1 shale stratigraphy coincides exactly with the occurrence of a grey carbonate band (Fig. 1 of Anbar et al., 2007). The findings from the Arctic Bay Formation suggest that secondary enrichment in Mo may be an alternative explanation for the high Mo/Al ratios in the McRae shale. In the present case, it is possible to test the origin of the metal enrichment because of the wide array of reported chemical data. Many black shale chemistry datasets that are used to make global-scale inferences do not report the full suite of metal concentrations, which means that the possible role of diagenetic overprinting cannot be assessed.

8. SUMMARY

Rare-earth elements and redox-sensitive metals together with lithostratigraphic analysis indicate that late Mesoproterozoic black shale of the Arctic Bay Formation (1092±59 Ma; Th-U-Pb whole-rock) was deposited under a stratified oxidised-euxinic water mass in an actively extensional basin. The highly redox-sensitive metals, such as Mo, V and U, were strongly enriched into the black shale and show coherent behaviour. These elements were probably supplied from the water column via a particle shuttle as well as possibly from diffuse venting. Less redox-sensitive metals (e.g., Zn and Ni) were also enriched, but to a lesser extent, and may not have been carried by a shuttle. The association of metal enrichment with dolomite content indicates either that the dolomite (or its precursor) was the shuttle,/or that secondary redistribution of metal resulted in enrichment in the most dolomitic shale horizons. Although there is no evidence for pronounced base-metal enrichment caused by SEDEX-type venting at the one black shale location studied in detail, the strong evidence of a chemocline and the establishment of bottom-water euxinia indicates that the geochemical conditions necessary for metal precipitation were present. Black shale of the Arctic Bay Formation was deposited during what appears to have been a global nadir of SEDEX/CD deposit formation, but its basin would have been geochemically capable of precipitating and concentrating base metals had they been supplied at a sufficient rate. The Shale Valley Central dataset provides insight into the complexity of water and sediment chemistry evolution in a restricted basin but cannot be used to infer global oceanic conditions.

8. ACKNOWLEDGEMENTS

Field work for this study was supported by Canada-Nunavut Geoscience Office, Polar Continental Shelf Project (Natural Resources Canada), and an NSERC Discovery Grant to ECT. The analytical work was covered by a Canada Research Chair award to BSK. Kristina Skeries is thanked for laboratory sample preparation, trace element analysis, and performing Pb purification. Harold Gibson contributed valuable suggestions regarding interpretation of the metal data. Celine Gilbert provided excellent assistance and companionship in the field. S. Piercey, K. Kelley, T. Algeo and an anonymous reviewer provided exceptionally helpful reviews; any remaining deficiencies of this study remain the responsibility of the authors.

REFERENCES

Algeo, T.J., Tribovillard, N., 2009. Environmental analysis of paleoceanographic systems based on molybdenum-uranium covariation. Chemical Geology 268, 211-225.

Anbar, A D., Duan, Y., Lyons, T.W., Arnold, G.L., Kendall, B., Creaser, R.A., Kaufman, A.J., Gordon, G.W., Scott, C., Garvin, J., Buick, R., 2007. A whiff of oxygen before the Great Oxidation Event? Science 317, 1903-1906.

Bau, M., Koschinsky, A., 2009. Oxidative scavenging of cerium on hydrous Fe oxide; evidence from the distribution of rare earth elements and yttrium between Fe oxides and Mn oxides in hydrogenetic ferromanganese crusts. Geochemical Journal 43, 37-47.

Byrne, R.H., Liu, X.W., Schijf, J., 1996. The influence of phosphate coprecipitation on rare earth distributions in natural waters. Geochimica et Cosmochimica Acta, 60, 3341-3346.

Calvert, S.E., Price, N.B., 1977. Geochemical variation in ferromanganese nodules and associated sediments from the Pacific Ocean. Marine Chemistry 5, 43-74.

Canfield, D.E., Poulton, S.W., Knoll, A.H., Narbonne, G.M., Ross, G., Goldberg, T., Strauss, H., 2008. Ferruginous conditions dominated later Neoproterozoic deep-water chemistry. Science 321, 949-952.

Cruse, A.M., Lyons, T.W., 2004. Sulfur and trace metal records of regional paleoenvironmental variability in Late Proterozoic black shales. Chemical Geology 206, 319-345.

Dahl, T.W., Canfield, D.E., Rosing, M.T., Frei, R.E., Gordon, G.W., Knoll, A.H., Anbar, A.D., 2011. Molybdenum evidence for expansive sulfidic water masses in similar to 750 Ma oceans. Earth and Planetary Science Letters 311, 264-274.

Denyszyn, S.W., Davis, D.W., Halls, H.C., 2009. Paleomagnetism and U-Pb geochronology of the Clarence Head dikes, Arctic Canada: orthogonal emplacement of mafic dikes in a large igneous province: Canadian Journal of Earth Sciences 46, 155-167.

Dostal, J., Jackson, G.D., Galley, A.G., 1989. Geochemistry of Neohelikian Nauyat plateau basalts, Borden rift basin, northwestern Baffin Island, Canada. Canadian Journal of Earth Sciences 26, 2214-2223.

Fahrig, W.F., Christie, K.W. and Jones, D.L., 1981. Paleomagnetism of the Bylot basins: evidence for Mackenzie continental tensional tectonics, *in* Campbell, F.H.A., ed., Proterozoic Basins of Canada: Geological Survey of Canada Paper 81-10, 303-312.

Galley, A.G., Jackson, G.D., Iannelli, T.R., 1983. Neohelikian subaerial basalts with ocean floor-type chemistry, northwestern Baffin Island (abstract): Geological Association of Canada, Program with Abstracts 8, A25.

Goodfellow, W.D., 2007. Base metal metallogeny of the Selwyn Basin, Canada, in: Goodfellow, W.D. (Ed.), Mineral Deposits of Canada. Geological Association of Canada Special Publication 5, pp. 553-579.

Goodfellow, W.D., Lydon, J.W., 2007. Sedimentary exhalative (SEDEX) deposits, in: Goodfellow, W.D. (Ed.), Mineral Deposits of Canada. Geological Association of Canada Special Publication 5, pp. 163-183.

Goodfellow, W.D., Lydon, J.W., Turner, R.J.W., 1993. Geology and genesis of stratiform sediment-hosted (SEDEX) zinc-lead-silver sulphide deposits, in: Kirkham, R.V., Sinclair, W.D., Thorpe, R.I. and Duke, J.M. (Eds.), Mineral Deposit Modeling. Geological Association of Canada Special Paper 40, pp. 201-251.

Heaman, L.M., LeCheminant, A.N., Rainbird, R.H., 1992. Nature and timing of Franklin igneous events, Canada: Implications for a Late Proterozoic mantle plume and the breakup of Laurentia. Earth and Planetary Science Letters 109, 117-131.

Hulbert, T.L.J., Carne R.C., Gregoire, D. C., Paktunc, D., 1992. Sedimentary nickel, zinc, and platinum group element mineralization in Devonian black shales, Nick Basin, Yukon, Canada: A new environment and deposit type. Exploration and Mining Geology 1, 39-62.

Jackson, G.D., Cumming, L.M., 1981. Evaporites and folding in the Neohelikian Society Cliffs Formation, northeastern Bylot Island, Arctic Canada. Geological Survey of Canada Paper 81-1C, 35-44.

Jackson, G.D., Iannelli, T.R. 1981. Rift-related cyclic sedimentation in the Neohelikian Borden basin, northern Baffin Island. Geological Survey of Canada Paper 81-10, 269-302.

Jackson, G.D., Morgan, W.C., 1978. Precambrian metamorphism on Baffin and Bylot islands, in: Fraser, J.A. and Heywood, W. (Eds.), Metamorphism in the Canadian shield. Geological Survey of Canada Paper 78-10, pp. 249-267.

Kah, L.C., Sherman, A.G., Narbonne, G.M., Knoll, A.H., Kaufman, A.J. 1999. $\delta^{13}C$ stratigraphy of the Proterozoic Bylot Supergroup, Baffin Island: implications for regional lithostratigraphic correlations. Canadian Journal of Earth Sciences 36**,** 313-332.

Kah, L.C., Lyons, T.M., Chelsey, J.T. 2001. Geochemistry of a 1.2 Ga carbonate-evaporite succession, northern Baffin and Bylot islands: implications for Mesoproterozoic marine evolution. Precambrian Research 111, 203-234.

Kamber, B.S., 2010. Archean mafic-ultramafic volcanic landmasses and their effect on ocean atmosphere chemistry. Chemical Geology 274, 19-28.

Kamber, B.S., 2009. Geochemical fingerprinting; 40 years of analytical development and real world applications. Applied Geochemistry 24, 1074-1086.

Kamber, B.S., Gladu, A.H., 2009. Comparison of Pb purification by anion-exchange resin methods and assessment of long-term reproducibility of Th/U/Pb ratio measurements by quadrupole ICP-MS. Geostandards and Geoanalytical Research 33, 169-181.

Kamber B.S., Bolhar, R., Webb, G.E., 2004. Geochemistry of late Archaean stromatolites from Zimbabwe: Evidence for microbial life in restricted epicontinental seas. Precambrian Research 132, 379-399.

Kamber B.S., Greig A., Collerson, K.D., 2005. A new estimate for the composition of weathered young upper continental crust from alluvial sediments, Queensland, Australia. Geochimica et Cosmochimca Acta 69, 1041-1058.

Knight, R.D., Jackson, G.D., 1994. Sedimentology and stratigraphy of the Mesoproterozoic Elwin Subgroup (Aqigilik and Sinasiuvik formations), uppermost Bylot Subgroup, Borden rift basin, northern Baffin Island. Geological Survey of Canada, Bulletin 455.

Kramers, J.D., Tolstikhin, I.N., 1997. Two terrestrial lead isotope paradoxes, forward transport modelling, core formation and the history of the continental crust. Chemical Geology 139, 75-110.

Leach, D.L., Sangster, D.F., Kelley, K.D., Large, R.R., Garven, G., Allen, C.R., Gutzmer, J., Walters, S., 2005. Sediment-hosted lead-zinc deposits: a global perspective. Economic Geology 100th Anniversary volume, 561-607.

Leach, D.L., Bradley, D.C., Huston, D., Pisarevsky, S.A., Taylor, R.D., Gardoll, S.J., 2010. Sediment-hosted lead-zinc deposits in Earth history. Economic Geology 105, 593–625.

LeCheminant, A.N., Heaman, L.M. 1989. Mackenzie igneous events, Canada: Middle Proterozoic hotspot magmatism associated with ocean opening. Earth and Planetary Science Letters 96, 38-48.

Leventhal, J.S., 1991. Comparison of organic geochemistry and metal enrichment in two black shales: Cambrian Alum Shale of Sweden and Devonian Chattanooga Shale of the United States. Mineralium Deposita 26, 104-112.

Long, D.G.F., Turner, E.C., in press. Tectonic, sedimentary and metallogenic re-evaluation of basal strata in the Mesoproterozoic Bylot basins (NU): are unconformity-type U concentrations a realistic expectation? Precambrian Research.

Lyons, T.W., Anbar, A.D., Severmann, S., Scott, C., Gill, B.C., 2009. Tracking euxinia in the ancient ocean: a multiproxy perspective and Proterozoic case study. Annual Review of Earth and Planetary Sciences 37, 507-534.

Marx, S.K., Kamber, B.S., 2010. Trace-element systematics of sediments in the Murray-Darling Basin, Australia: Sediment provenance and palaeoclimate implications of fine scale chemical heterogeneity. Applied Geochemistry 25, 1221-1237.

Mazzullo, S.J., 2000. Organogenic dolomitization in peritidal to deep-sea sediments. Journal of

Sedimentary Research 70, 10-23.

Murphy, D.T., Kamber, B.S., Collerson, K.D., 2003. A refined solution to the first terrestrial Pb-isotope paradox. Journal of Petrology 44, 39-53.

Ohta, A., Ishii, S., Sakakibara, M., Mizuno, A., Kawabe, I., 1999. Systematic correlation of the Ce anomaly with the Co/(Ni+Cu) ratio and Y fractionation from Ho in distinct types of Pacific deep-sea nodules. Geochemical Journal 33, 399-417.

Pehrsson, S.J., Buchan, K.L., 1999. Borden dykes of Baffin Island, N.W.T.: A Franklin U-Pb baddeleyite age and a paleomagnetic interpretation. Canadian Journal of Earth Sciences 36, 65-73.

Raiswell, R., Reinhard, C.T., Derkowski, A., Owens, J., Bottrell, S.H., Anbar, A.D., Lyons, T.W., 2011. Formation of syngenetic and early diagenetic iron minerals in the late Archean Mt. McRae Shale, Hamersley Basin, Australia: New insights on the patterns, controls and paleoenvironmental implications of authigenic mineral formation. Geochimica et Cosmochimica Acta 75, 1072-1087.

Russell, M.J., Solomon, M., Walshe, J.L., 1981. The genesis of sediment-hosted, exhalative zinc and lead deposits. Mineralium Deposita 16, 113-127.

Rooney, A.D., Selby, D., Houzay, J.-P., Renne, P.R., 2010. Re-Os geochronology of a Mesoproterozoic sedimentary succession, Taoudeni basin, Mauritania: Implications for basin-wide correlations and Re-Os organic-rich sediment systematics. Earth and Planetary Science Letters 289, 486-496.

Scott, D.J., deKemp, E.A., 1998. Bedrock geology compilation, northern Baffin Island and northern Melville Peninsula. Geological Survey of Canada Open File 3633.

Scott, C., Lyons, T.W., Bekker, A., Shen, Y. Poulton, S.W., Chu, X., Anbar, A.D., 2008. Tracing the stepwise oxygenation of the Proterozoic ocean. Nature 452, 456-459.

Sherman, A.G., James, N.P., Narbonne, G.M. 2002. Evidence for reversal of basin polarity during carbonate ramp development in the Mesoproterozoic Borden Basin, Baffin Island. Canadian Journal of Earth Sciences 39, 519-538.

Turner, E.C., 2004. Origin of basinal carbonate laminites of the Mesoproterozoic Society Cliffs Formation (Borden Basin, Nunavut), and implications for base metal mineralisation. Geological Survey of Canada Current Research 2004-B2, 12 p.

Turner, E.C., 2009. Mesoproterozoic carbonate systems in the Borden Basin, Nunavut. Canadian Journal of Earth Sciences 46, 915-938.

Turner, E.C., 2011. Structural and stratigraphic controls on carbonate-hosted base-metal mineralization in the Mesoproterozoic Borden Basin (Nanisivik District), Nunavut. Economic Geology 106, 1197-1223.

Ulrich, T. Kamber, B.S., Woodhead, J.D., Spencer, L.A. 2010. Long-term observations of isotope ratio accuracy and reproducibility using quadrupole ICP mass spectrometry. Geostandards and Geoanalytical Research 34, 161-174.

Webb, G.E., Nothdurft, L.D., Kamber, B.S., Kloprogge, J.T., Zhao, J.X., 2009. Rare earth element geochemistry of scleractinian coral skeleton during meteoric diagenesis: a sequence through neomorphism of aragonite to calcite. Sedimentology 56, 1433-1463.

Xu, Y.G., Ma, J.L., Frey, F.A., Feigenson, M.D., Liu, J.F., 2005. Role of lithosphere-asthenosphere interaction in the genesis of Quaternary alkali and tholeiitic basalts from Datong, western North China Craton. Chemical Geology 224, 247-271.

FIGURE CAPTIONS

Fig. 1. (A) Two study locations (black stars) on a tectonic map of the Borden Basin, of which the main trough is the Milne Inlet Graben. Only the three formations relevant to base-metal prospectivity are shown (other parts of the Bylot Supergroup, as well as crystalline basement and Paleozoic strata are shown in grey). (B) Location of Borden Basin among the other Bylot basins. (C) Location of map (A) in Canada's Arctic islands.

Fig. 2. (A) Generalised stratigraphy of the Bylot Supergroup, after Jackson and Iannelli (1981), Sherman et al. (2002), and Turner (2009), including tectonostratigraphic interpretation and diagrammatic depiction of geometric complexity among Arctic Bay Formation (grey & black fill) and associated carbonate formations. IQ = Iqqittuq Fm.; AT = Angmaat Fm.; IK = Ikpiarjuk Fm.; NA = Nanisivik Fm.; FF = Fabricius Fiord Fm. The Fabricius Fiord Formation is present only along the margins of the Milne Inlet Graben. (B) Stratigraphic panel of part of the Arctic Bay Formation with proposed correlations for the two localities (Shale Valley (SV) and Alpha River (AR)) addressed in this study. Vertical bars to right of stratigraphic column indicate iridescent weathering sheen (grey) and rusty weathering (black) in field exposures. Note scale difference between SV and AR. (C) Expanded view of two sections at Shale Valley (SV Central and East), showing inferred synsedimentary truncation surface, lateral thickness and facies changes, and relationship to the overlying flank of a carbonate mound. Four lithostratigraphic units are identified in the two areas: (1) siltstone and sandstone of a northwest-deepening storm-dominated ramp; (2) sub-storm-wave-base siltstone with rare but conspicuous carbonate nodules; (3) black shale with subtle grain-size cycles; and (4) black shale with early diagenetic discoidal

calcite concretions, sooty carbonate layers, and debrites of clasts of these lithofacies. SVC and SVE are separated by 5 km, but had distinctly different sedimentary histories because of sea-floor topography associated with syndepositional activity of a nearby fault, as well as owing to their different proximities to the tapering flank of an Ikpiarjuk Fm. carbonate mound in the uppermost parts of the sections.

Fig. 3. Field exposures of Arctic Bay Formation and associated strata. (A) Shale Valley Central (SVC) section in westernmost Milne Inlet Graben, with C. Gilbert in foreground. Section SVC follows gully in centre of photo. The lower part of the Arctic Bay Formation is not exposed. (B) Arctic Bay Fm. as exposed on northeast side of Alpha River Valley near Tremblay Sound. Contact with underlying Adams Sound Fm. is just above river level. The geometric relationships among Arctic Bay Formation and overlying carbonate units of the southeastern (Iqqittuq and Angmaat fms.) and northwestern Milne Inlet Graben (Ikpiarjuk and Nanisivik fms.) are displayed. The uppermost Arctic Bay Formation is laterally equivalent to the upper part of the outermost Iqqittuq Fm. (carbonate ramp) and also to deep-water carbonate mounds of the Ikpiarjuk Fm. Section AR follows red dashed line. Strata dip away from viewer at various attitudes between 10° and 20°. Elevation difference between valley bottom and plateau is approximately 550 m. (C) An intraformational truncation surface (ITS; healed low-angle slope-failure scar) in the Arctic Bay Formation at on south wall of Shale Valley records syndepositional tectonic activity: gravitational failure of a shale slope and healing of the scar by continued shale deposition. The eastward down-cutting truncation direction is opposite to the overall gentle northwestward deepening of the basin, supporting the idea of local slope development associated with nearby syndepositional fault activity. (D) Subtle ITS in the

outermost ramp strata of the Iqqittuq Fm. on the south wall of Alpha River Valley, near where Iqqittuq Fm. passes laterally to upper Arctic Bay Fm. Eastward down-cutting is antithetical to the overall westward deepening indicated by lithostratigraphic pattern, attesting to the presence of a local slope caused by movement on a rift-related intra-graben fault (the Tikirarjuaq Fault Zone is in the valley toward the viewer). Exposure is approximately 500 m thick.

Fig. 4. Upper continental crust normalised (using MUQ of Kamber et al., 2005) REE patterns of non-shale samples analysed by ICP-MS. Panel A shows two siltstones (SVC-51 and 55) and one carbonate nodule (SVC-60) compared to representative sub-recent diagenetic central Pacific Mn nodules (average of samples HW-2 and HW-15 from Ohta et al., 1999). Panel B shows non-nodular carbonate samples. Panel C compares the most calcareous shale sample (SVC-80), average carbonate (from panel B) and a carbonate-free shale (SVC-86). For explanation see text.

Fig. 5. Upper continental crust normalised (using MUQ of Kamber et al., 2005) REE patterns of shale samples as function of stratigraphic height. Samples were grouped into 7 height intervals. Relative position is indicated by weight of shading. For explanation see text.

Fig. 6. (A) Correlation between measured 500-1000ºC LOI and that calculated when attributing all Ca and Mg in sample to carbonate (excepting the two Mn-rich siltstone nodules). (B) Correlation between carbonate content (approximated with CaO + MgO) and Y/Ho ratio. Note that calcite crystal concretion is shown as open circle and plots off the trend defined by the

shales. (C) A positive trend between Al_2O_3 content and sum of lanthanide concentration (note that this does not include Y) is found up to Al_2O_3 of 11.5 wt%, whereas in the more aluminous samples, REE content is not at all related to argillaceous content.

Fig. 7. Chemostratigraphic plots of samples, omitting siltstone and carbonate nodules. (A) Coherent stratigraphic patterns for Zr, Nb and Tm. (B) Stratigraphic trends defined by redox-sensitive elements U, Mo and Ni. (C) Plots of ratios of redox-sensitive metal relative to immobile lithophile element shows steady, strong enrichment in Mo, Cd and V from 50 m to a peak at 200 m before returning to low values above 250 m.

Fig. 8. Binary co-variation diagrams. (A) Strong positive correlation between relative V and Mo enrichment (see also Fig. 9C). (B) Moderately strong correlation is also found between relative U and Ni enrichments. (C) Very strong positive correlation between relative V enrichment and Y/Ho ratio. See explanation in text.

Fig. 9. Common Pb-isotope diagram showing 17 whole-rock data-points used for isochron calculation (solid small diamond symbols with 1-sigma error bars). Note two outliers (solid squares with error bars). For reference, the evolution lines (in 100 Ma steps) of depleted mantle (solid circles) and younger upper continental crust (open circles) are also shown up to 1200 Ma (after Kramers and Tolstikhin, 1997). Note that the isochron projects towards a composition approximately mid-way on the tie-line (stippled) between 1.2 Ga mantle and juvenile crust.

Fig. 10. Inboard (southeast) – outboard (northwest) schematic view of basin evolution during deposition of the Arctic Bay Fm., based on field lithostratigraphy. Southeastern one-third of the MIG is not shown. (1) During deposition of the lowermost Arctic Bay Fm., the MIG deepened northwestward, the sea-floor was above storm wave-base everywhere, and sediment consisted of quartz sand and silt. At graben margins (not shown), wedges of coarse terrigenous debris began to be deposited (Fabricius Fiord Fm.). (2) The sea-floor deepened and the northwestern MIG was dominated by silt deposited below storm wave-base. Carbonate layers were deposited, diagenetically altered in the subsurface, and locally redeposited as intraclast rudstone. (3) After continued deepening and development of a chemocline, the MIG northwest of Alpha River became a black shale basin. The AR location may also have experienced black shale deposition during intervals recorded by sedimentary rocks now obscured by cover. Geochemical data indicate that the clay was supplied by weathering of exposed basalt (Nauyat Fm.) (4) During deposition of the upper part of the black shale across the central and western MIG, millimetric discoidal calcite concretions grew below the sediment-water interface. Shale Valley was near a locus of deep-water mound development (Ikpiarjuk Fm.), and sooty carbonate, slumps and concretion-clast debrites near the top of the formation are related lithofacies. Syndepositional fault activity is indicated throughout black shale deposition by ITSs at this locality. (5) Abrupt but conformable transition to terrigenous-free dolostone laminite of the Nanisivik Fm. reflects regional tectonic adjustment of the basin and elimination of clay supply (see Turner, 2004 and Turner, 2009). Fabricius Fiord Fm. continues to be deposited at graben margins (not shown; Jackson and Iannelli, 1981).

TABLE CAPTIONS

Table 1. Major element, four-step loss-on-ignition, RockEval, trace element, and Pb-isotope data.

Table 1: Major element, total organic carbon and loss on ignition (wt%), trace element (ppb) anc

	09-SVC-51	09-SVC-53	09-SVC-55	09-SVC-58	09-SVC-60	09-SVC-62
Height (m)	5.5	12	23	31.5	44	66
Type	FeMn nodule	Rusty sst	FeMn nodule	Shale (calc)	Carb nod	Rusty shale
SiO_2	31.37	63.96	42.67	59.34		54.56
TiO_2	0.22	0.3	0.37	0.86		0.73
Al_2O_3	6.12	9.1	10.23	19.78		16.23
Fe_2O_3	33.23	10.66	21.51	6.14		4.03
MnO	2.14	0.55	0.89	0.02		0.01
MgO	2.46	2.58	2.48	2.01		1.28
CaO	2.06	3.74	5.89	0.24		0.31
Na_2O	0.3	1.33	0.4	0.47		1.25
K_2O	0.8	0.64	1.02	4.7		2.89
P_2O_5	1.05	0.01	4.33	0.06		0.07
LOI	20.17	7.29	9.95	6.56		18.45
SO_3						
TOC	0.55	0.07	0.22	0.14		9.01
Total	99.93	100.15	99.75	100.19		99.81
N_2 (105°C)	0.39	0.23	0.51	1.73		2.11
O_2 (371°C)	0.4	0.22	0.66	0.55		1.5
O_2 (500°C)	0.52	0.12	0.59	0.26		11.43
O_2 (1000°C)	16.78	6.11	7.45	3.68		2.12
Total LOI	18.09	6.68	9.21	6.22		17.16
Li	33360	56510	82930	50760	47510	52220
Be	1454	2927	1763	4119	453	2405
Sc	4442	13130	11820	13620	6255	14520
Ti	875400	4944000	3613000	5221000	963700	4258000
V	23140	66300	50400	94440	17730	134000
Cr	14160	62910	42940	76190	16400	71710
Co	9516	27670	18470	11520	26150	2041
Ni	12970	28810	32160	32040	36290	45800
Cu	6445	10790	68340	bdl	1995	25330
Zn	45280	67960	1040000	53140	203300	18840
Ga	6952	23140	17550	28010	6907	23400
As	468	5165	1469	554	214	8102
Rb	29410	140300	82680	224600	12920	132600
Sr	34600	88910	116800	97230	101500	103200
Y	31590	45850	170300	33540	26110	31120
Zr	30450	262300	231500	168300	32820	152000
Nb	2816	17300	11850	17700	2722	11010
Mo	223	484	676	207	50	10440
Ag	19	201	51	27	12	424
Cd	16	94	338	57	69	64
In	23	94	475	71	23	33
Sn	133	3482	1453	5034	521	5001

Figure 1 colour

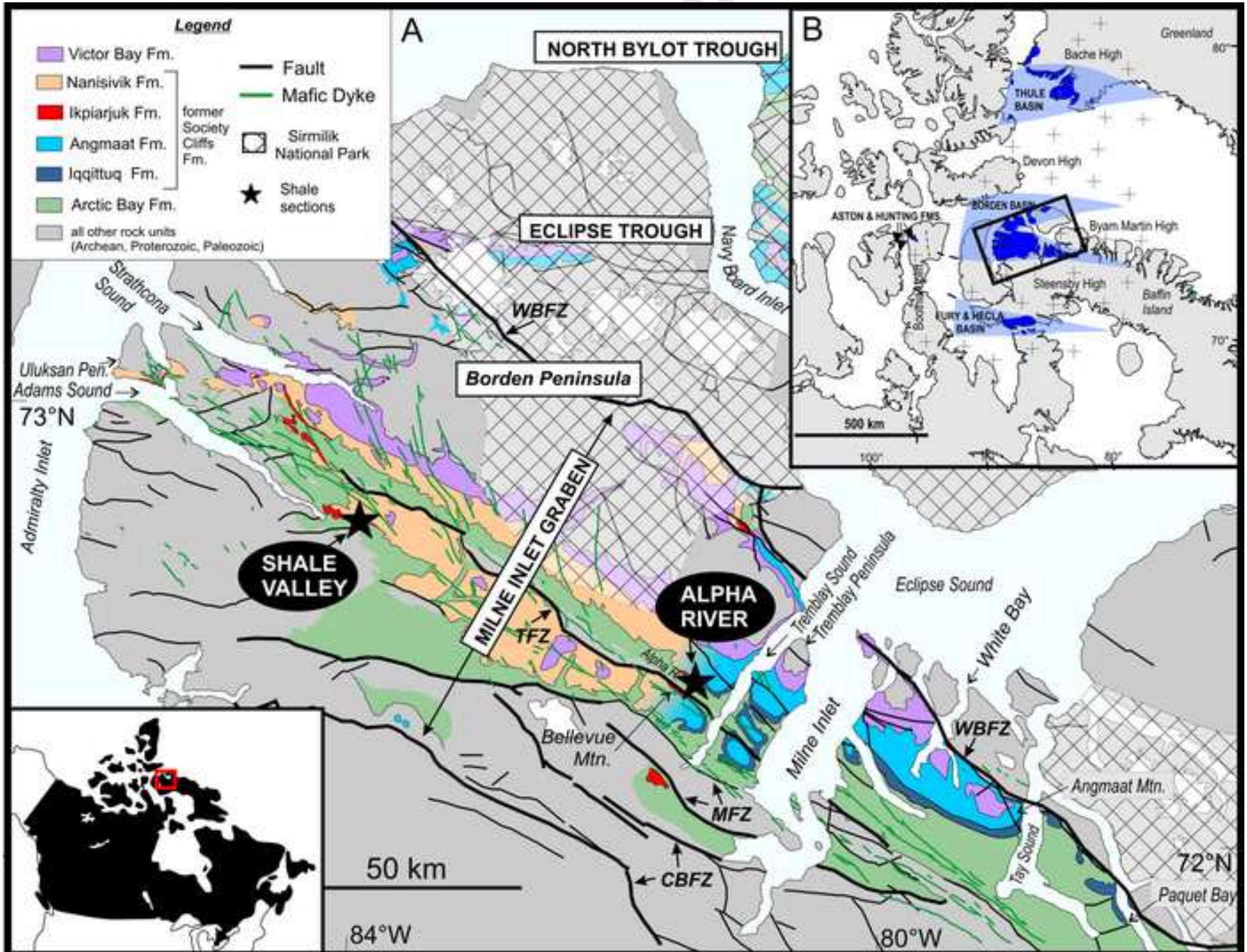

Figure 1 B&W

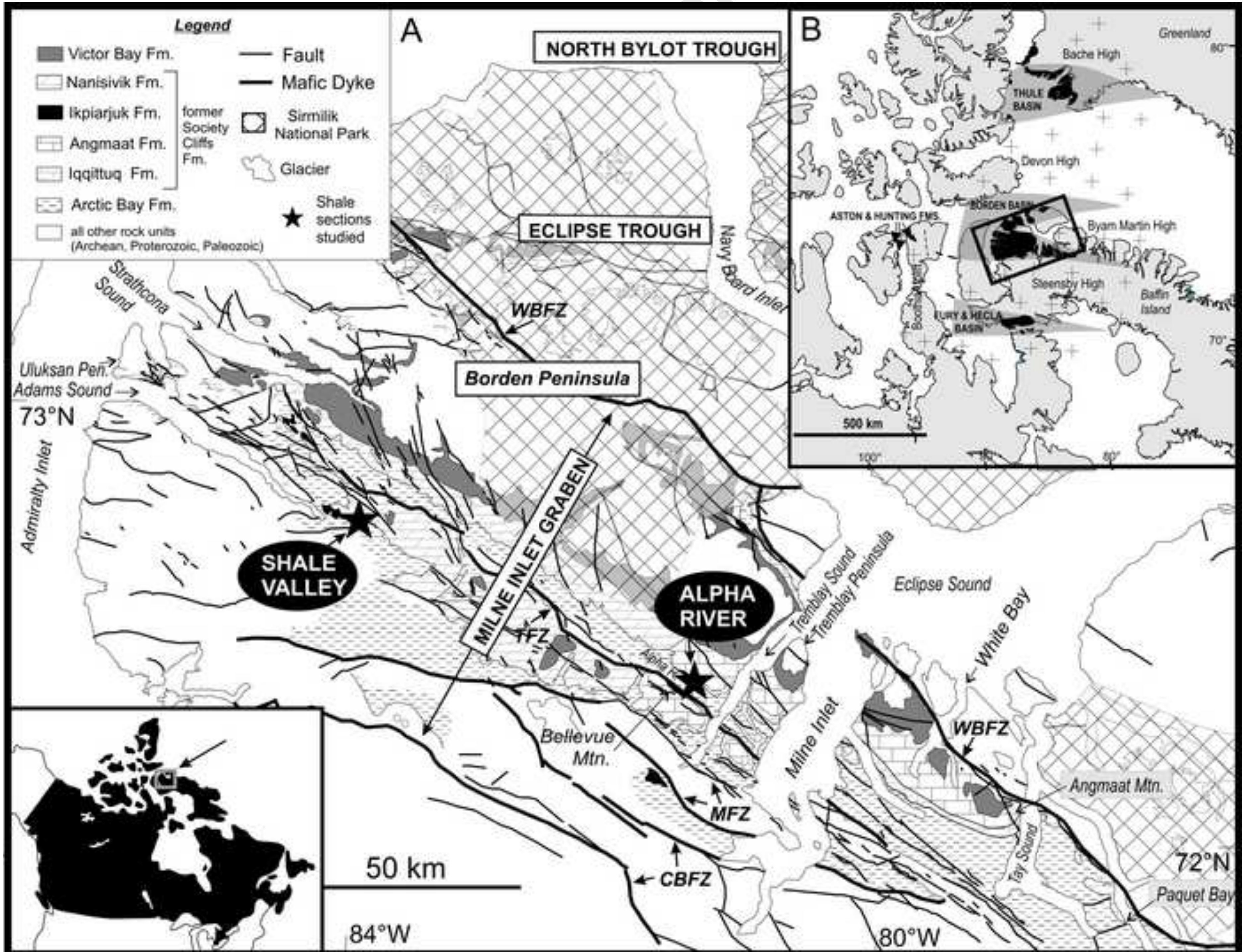
Legend
Victor Bay Fm.
Nanisivik Fm.
Ikpiarjuk Fm.
Angmaat Fm.
Iqqittuq Fm.
former Society Cliffs Fm.
Arctic Bay Fm.
all other rock units (Archean, Proterozoic, Paleozoic)
Fault
Mafic Dyke
Sirmilik National Park
Glacier
Shale sections studied
A
NORTH BYLOT TROUGH
ECLIPSE TROUGH
Navy Board Inlet
Strathcona Sound
WBFZ
Borden Peninsula
Uluksan Pen.
Adams Sound
73°N
Admiralty Inlet
MILNE INLET GRABEN
SHALE VALLEY
ALPHA RIVER
Tremblay Sound
Tremblay Peninsula
Eclipse Sound
White Bay
TFZ
Bellevue Mtn.
Milne Inlet
WBFZ
Angmaat Mtn.
MFZ
CBFZ
50 km
Tay Sound
72°N
Paquet Bay
84°W
80°W
B
Greenland
Bache High
THULE BASIN
Devon High
BORDEN BASIN
ASTON & HUNTING FMS.
Byam Martin High
Steensby High
Baffin Island
FURY & HECLA BASIN
500 km
100°
80°
70°

Figure 2

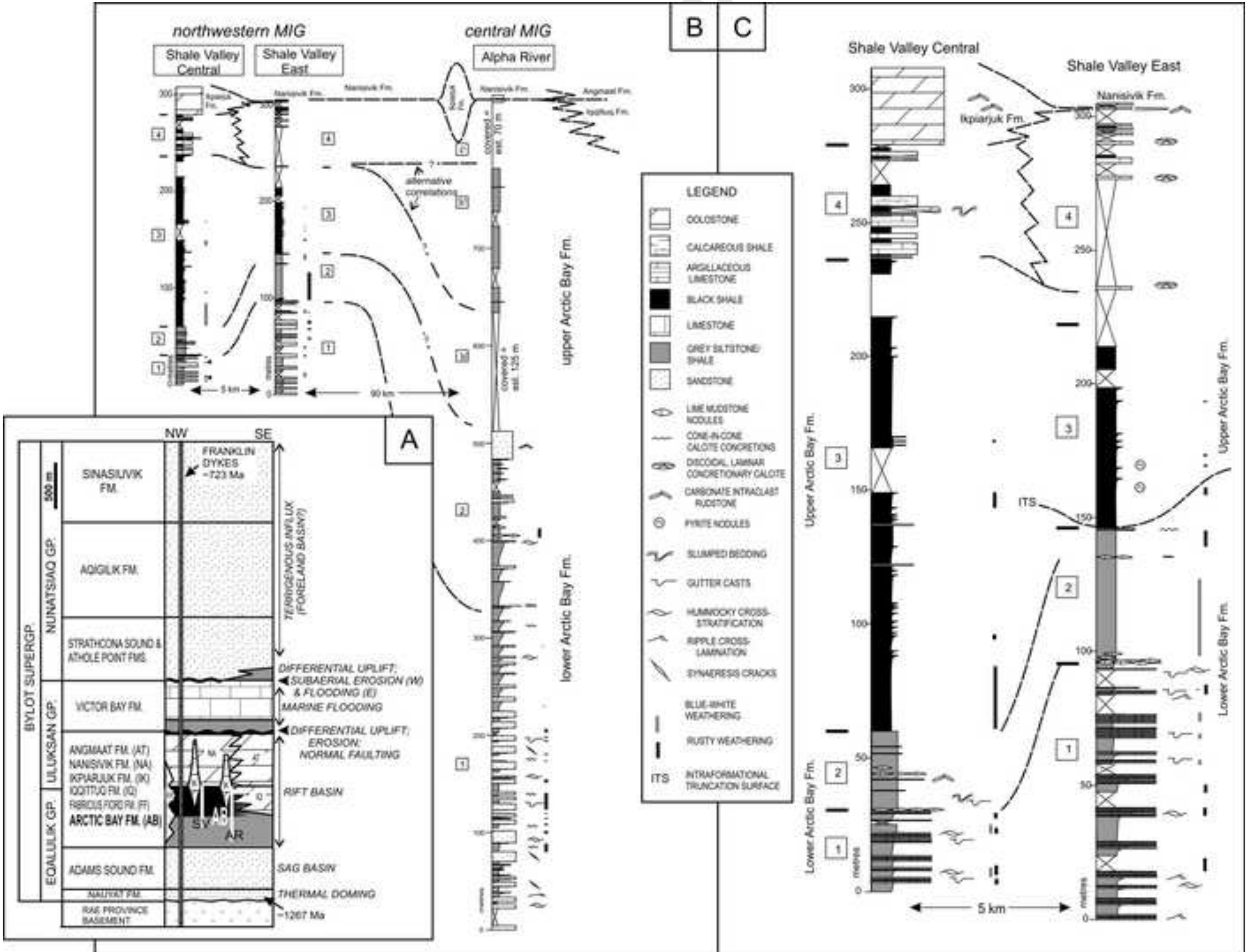
B
C
A
northwestern MIG
central MIG
Shale Valley Central
Shale Valley East
Alpha River
alternative correlations
upper Arctic Bay Fm.
lower Arctic Bay Fm.
5 km
90 km
LEGEND
DOLOSTONE
CALCAREOUS SHALE
ARGILLACEOUS LIMESTONE
BLACK SHALE
LIMESTONE
GREY SILTSTONE/ SHALE
SANDSTONE
LIME MUDSTONE NODULES
CONE-IN-CONE CALCITE CONCRETIONS
DISCOIDAL, LAMINAR CONCRETIONARY CALCITE
CARBONATE INTRACLAST RUDSTONE
PYRITE NODULES
SLUMPED BEDDING
GUTTER CASTS
HUMMOCKY CROSS-STRATIFICATION
RIPPLE CROSS-LAMINATION
SYNAERESIS CRACKS
BLUE-WHITE WEATHERING
RUSTY WEATHERING
ITS
INTRAFORMATIONAL TRUNCATION SURFACE
NW
SE
FRANKLIN DYKES ~723 Ma
BYLOT SUPERGP.
NUNATSIAQ GP.
ULUKSAN GP.
EQALULIK GP.
500 m
SINASIUVIK FM.
AQIGILIK FM.
STRATHCONA SOUND & ATHOLE POINT FMS.
VICTOR BAY FM.
ANGMAAT FM. (AT)
NANISIVIK FM. (NA)
IKPIARJUK FM. (IK)
IQQITTUQ FM. (IQ)
FABRICIUS FIORD FM. (FF)
ARCTIC BAY FM. (AB)
ADAMS SOUND FM.
NAUYAT FM.
RAE PROVINCE BASEMENT
SV
AR
TERRIGENOUS INFLUX (FORELAND BASIN?)
DIFFERENTIAL UPLIFT; SUBAERIAL EROSION (W) & FLOODING (E)
MARINE FLOODING
DIFFERENTIAL UPLIFT; EROSION; NORMAL FAULTING
RIFT BASIN
SAG BASIN
THERMAL DOMING
~1267 Ma
Nanisivik Fm.
Ikpiarjuk Fm.
Upper Arctic Bay Fm.
Lower Arctic Bay Fm.
metres

Figure 3 colour

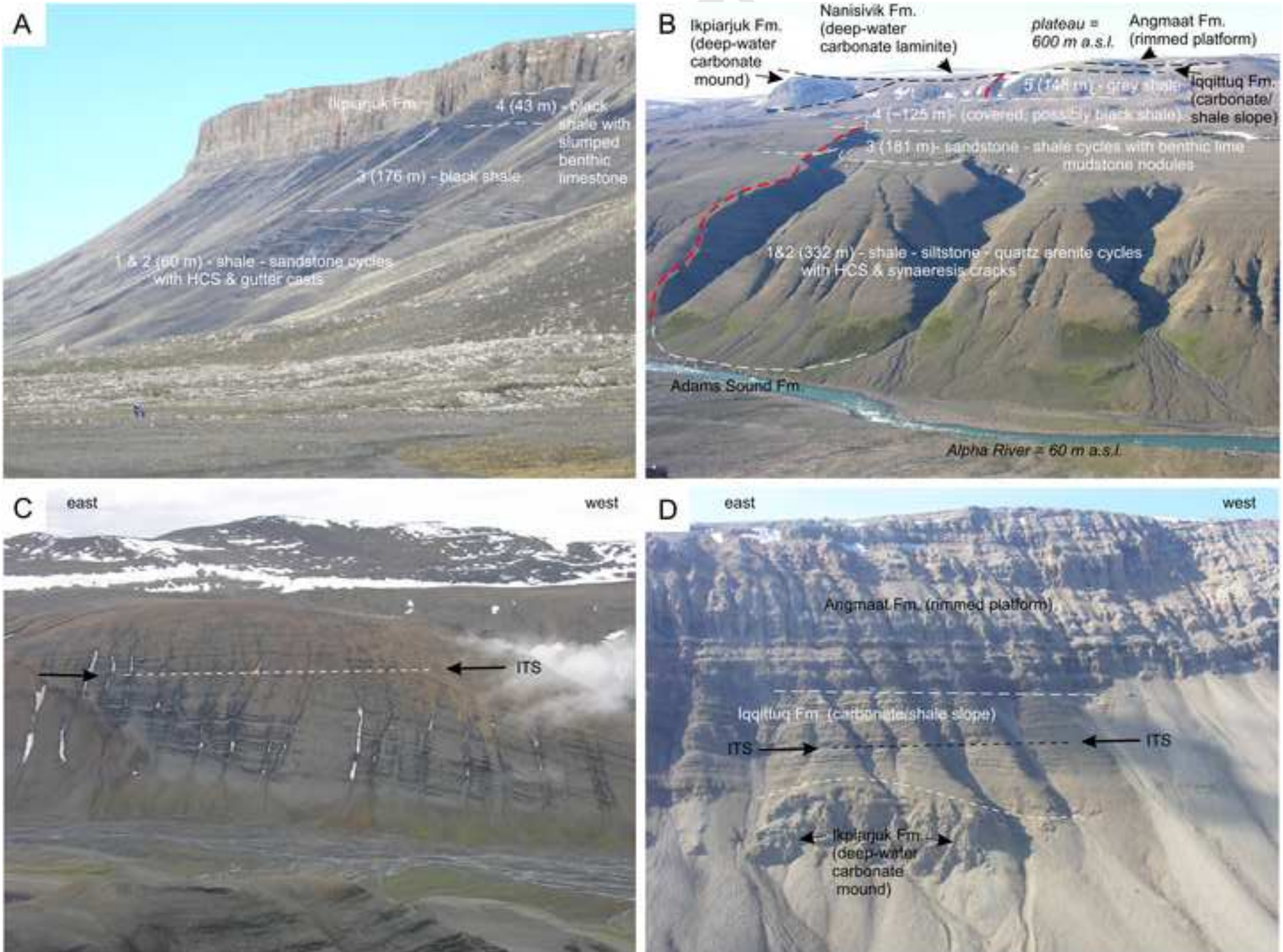

Figure 3 B&W

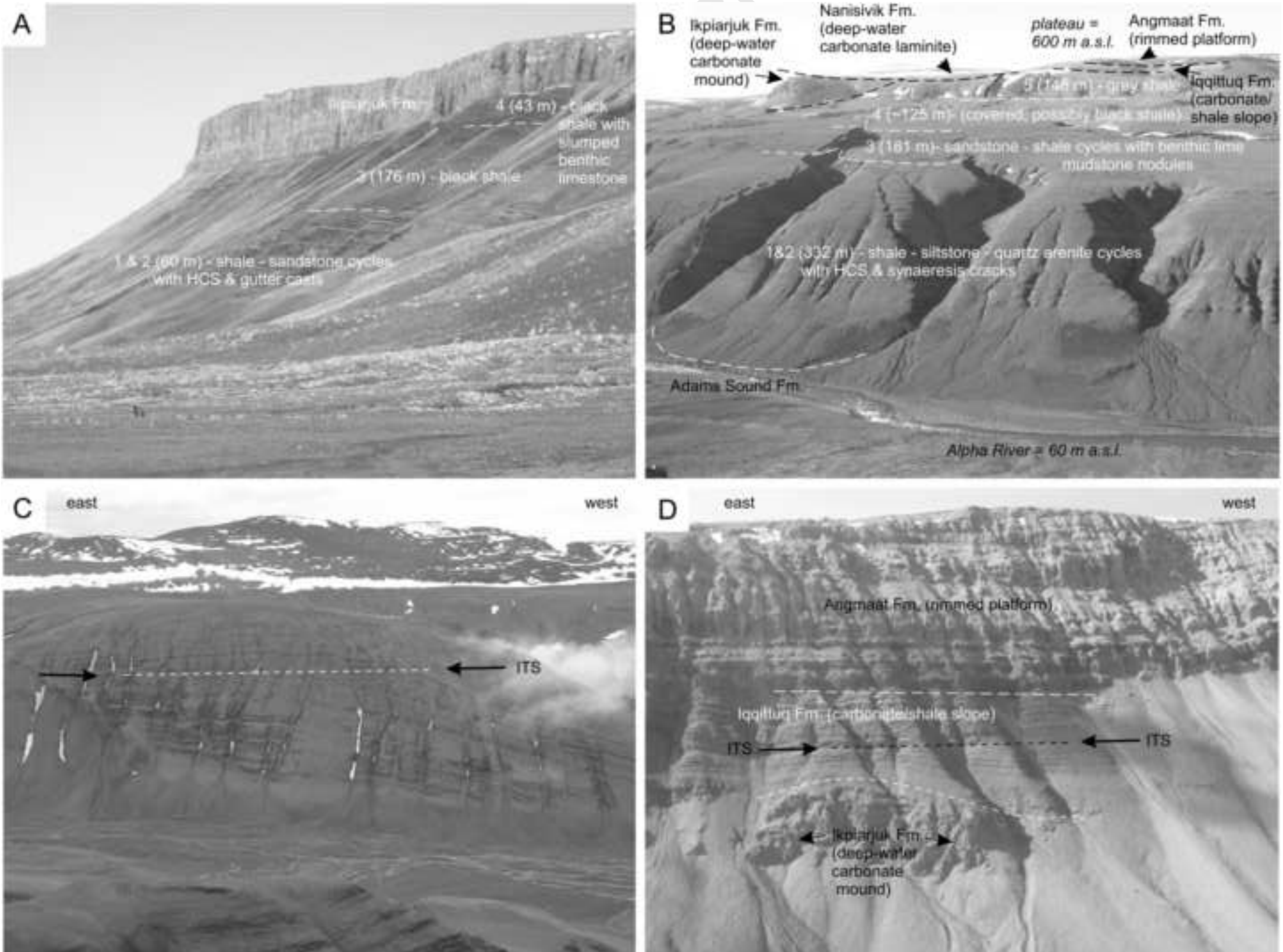
A
3 (176 m) - black shale
1 & 2 (60 m) - shale - sandstone cycles
with HCS & gutter casts
B
Ikpiarjuk Fm.
(deep-water
carbonate
mound)
Nanisivik Fm.
(deep-water
carbonate laminite)
plateau =
600 m a.s.l.
Angmaat Fm.
(rimmed platform)
Iqqittuq Fm.
(carbonate/
shale slope)
3 (161 m)- sandstone - shale cycles with benthic lime
mudstone nodules
1&2 (332 m) - shale - siltstone - quartz arenite cycles
with HCS & synaeresis cracks
Adams Sound Fm
Alpha River = 60 m a.s.l.
C
east
west
ITS
D
east
west
Angmaat Fm. (rimmed platform)
Iqqittuq Fm. (carbonate/shale slope)
ITS
ITS
Ikpiarjuk Fm.
(deep-water
carbonate
mound)

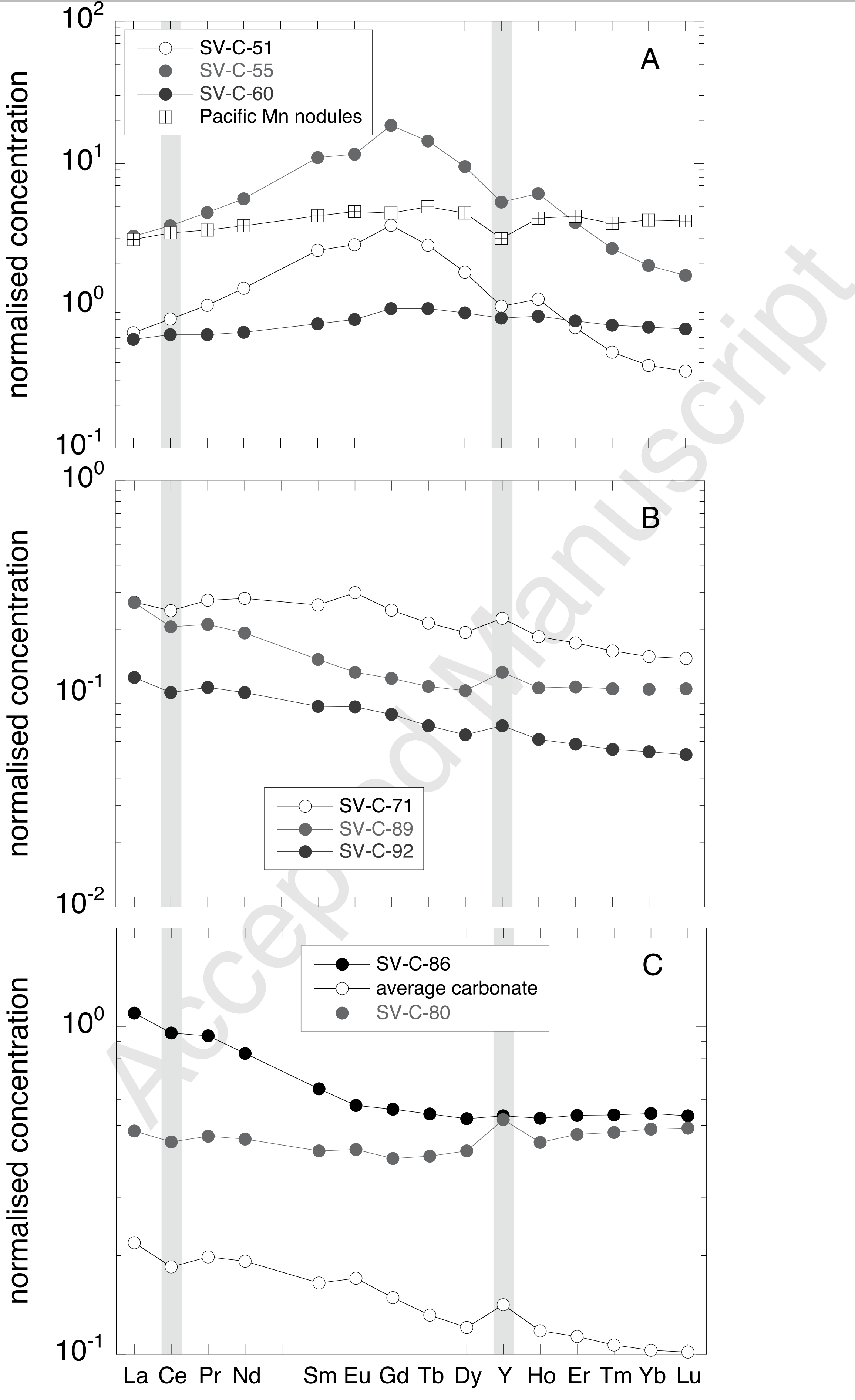
A
SV-C-51
SV-C-55
SV-C-60
Pacific Mn nodules
B
SV-C-71
SV-C-89
SV-C-92
C
SV-C-86
average carbonate
SV-C-80
normalised concentration
La
Ce
Pr
Nd
Sm
Eu
Gd
Tb
Dy
Y
Ho
Er
Tm
Yb
Lu

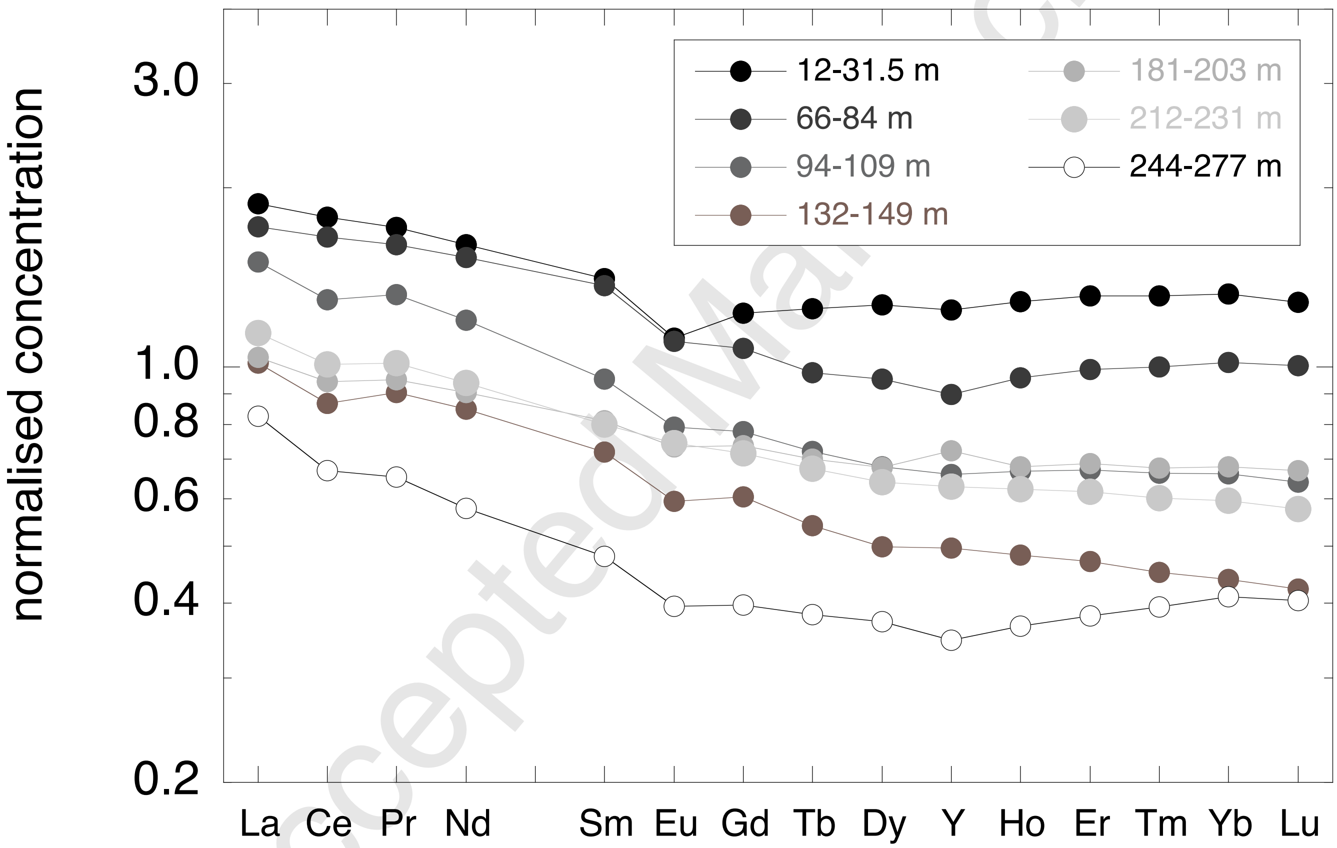
12-31.5 m
66-84 m
94-109 m
132-149 m
181-203 m
212-231 m
244-277 m
normalised concentration
3.0
1.0
0.8
0.6
0.4
0.2
La
Ce
Pr
Nd
Sm
Eu
Gd
Tb
Dy
Y
Ho
Er
Tm
Yb
Lu

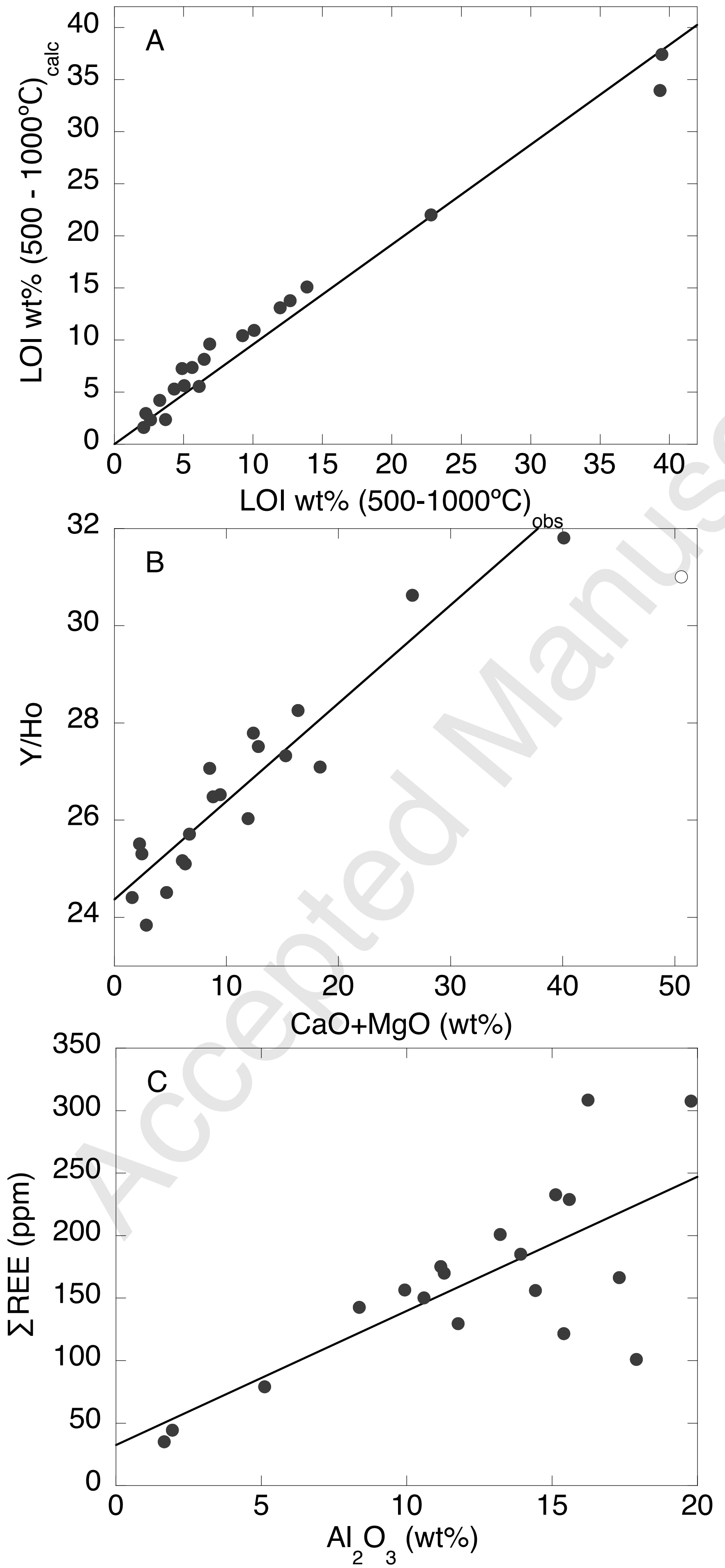

A
LOI wt% (500 - 1000ºC)calc
LOI wt% (500-1000ºC)obs
0
5
10
15
20
25
30
35
40
B
Y/Ho
CaO+MgO (wt%)
24
26
28
30
32
0
10
20
30
40
50
C
ΣREE (ppm)
Al2O3 (wt%)
0
50
100
150
200
250
300
350
0
5
10
15
20

Figure 7

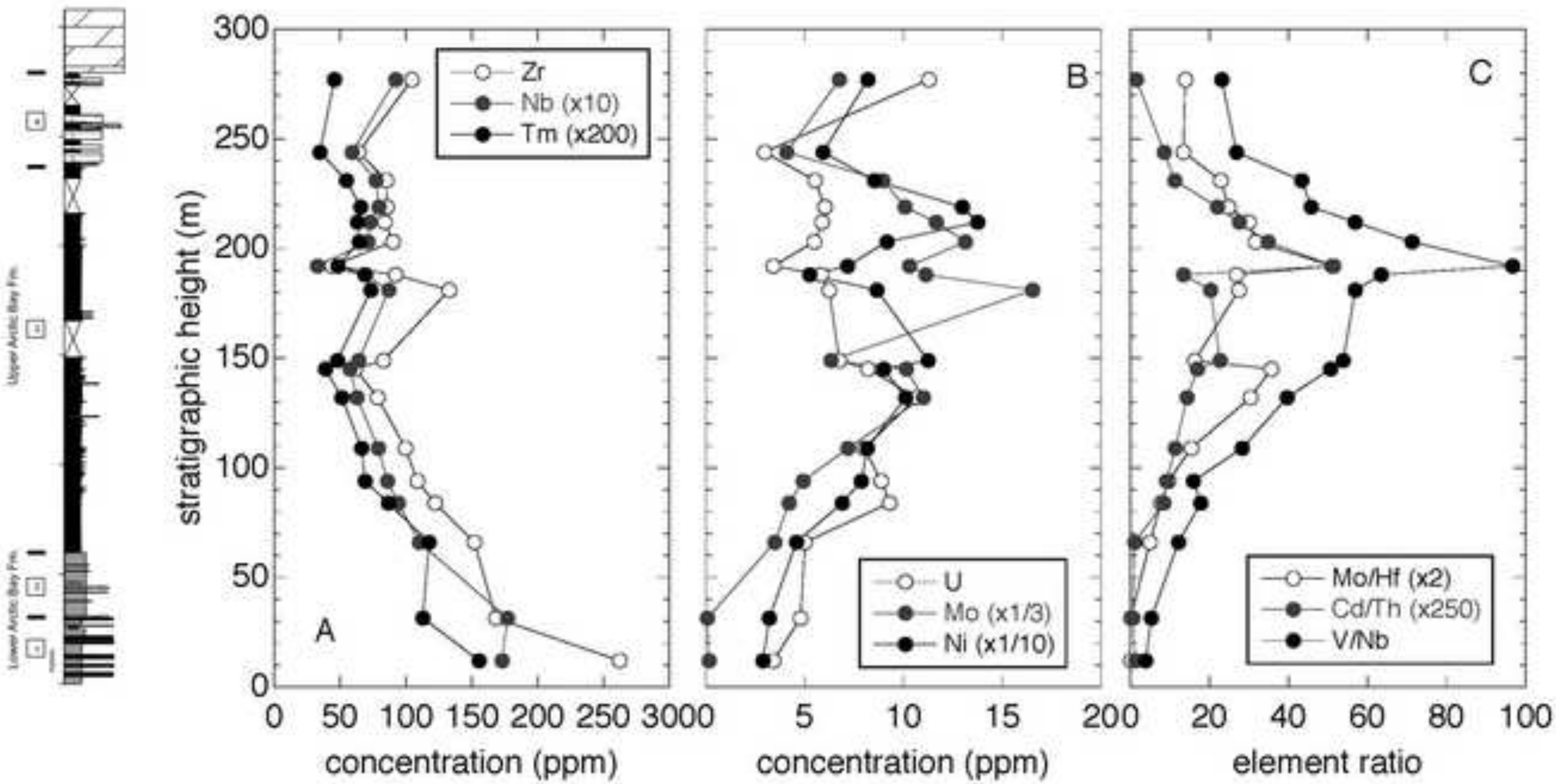
A
B
C
Zr
Nb (x10)
Tm (x200)
U
Mo (x1/3)
Ni (x1/10)
Mo/Hf (x2)
Cd/Th (x250)
V/Nb
stratigraphic height (m)
concentration (ppm)
concentration (ppm)
element ratio

Figure 8

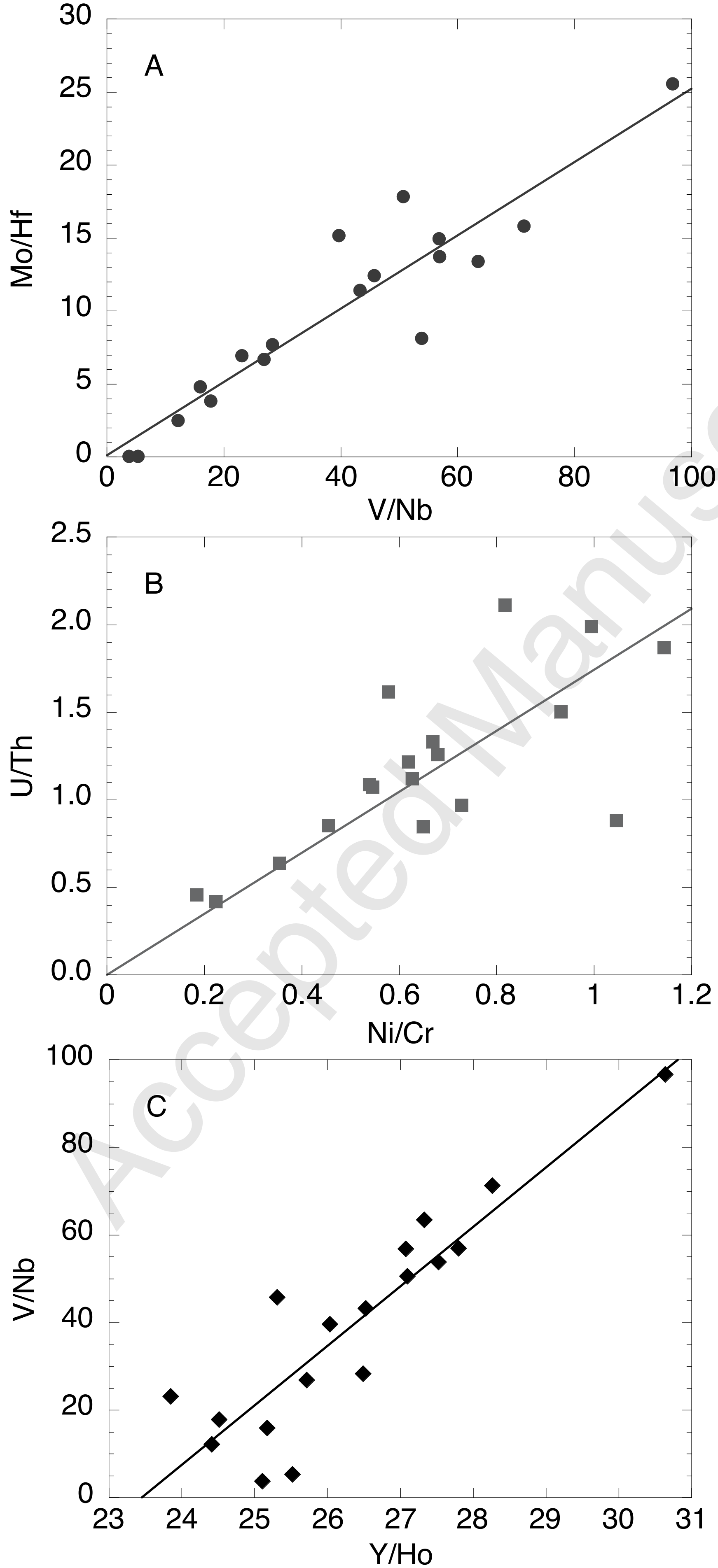
A
Mo/Hf
V/Nb
0
5
10
15
20
25
30
0
20
40
60
80
100
B
U/Th
Ni/Cr
0.0
0.5
1.0
1.5
2.0
2.5
0
0.2
0.4
0.6
0.8
1
1.2
C
V/Nb
Y/Ho
0
20
40
60
80
100
23
24
25
26
27
28
29
30
31

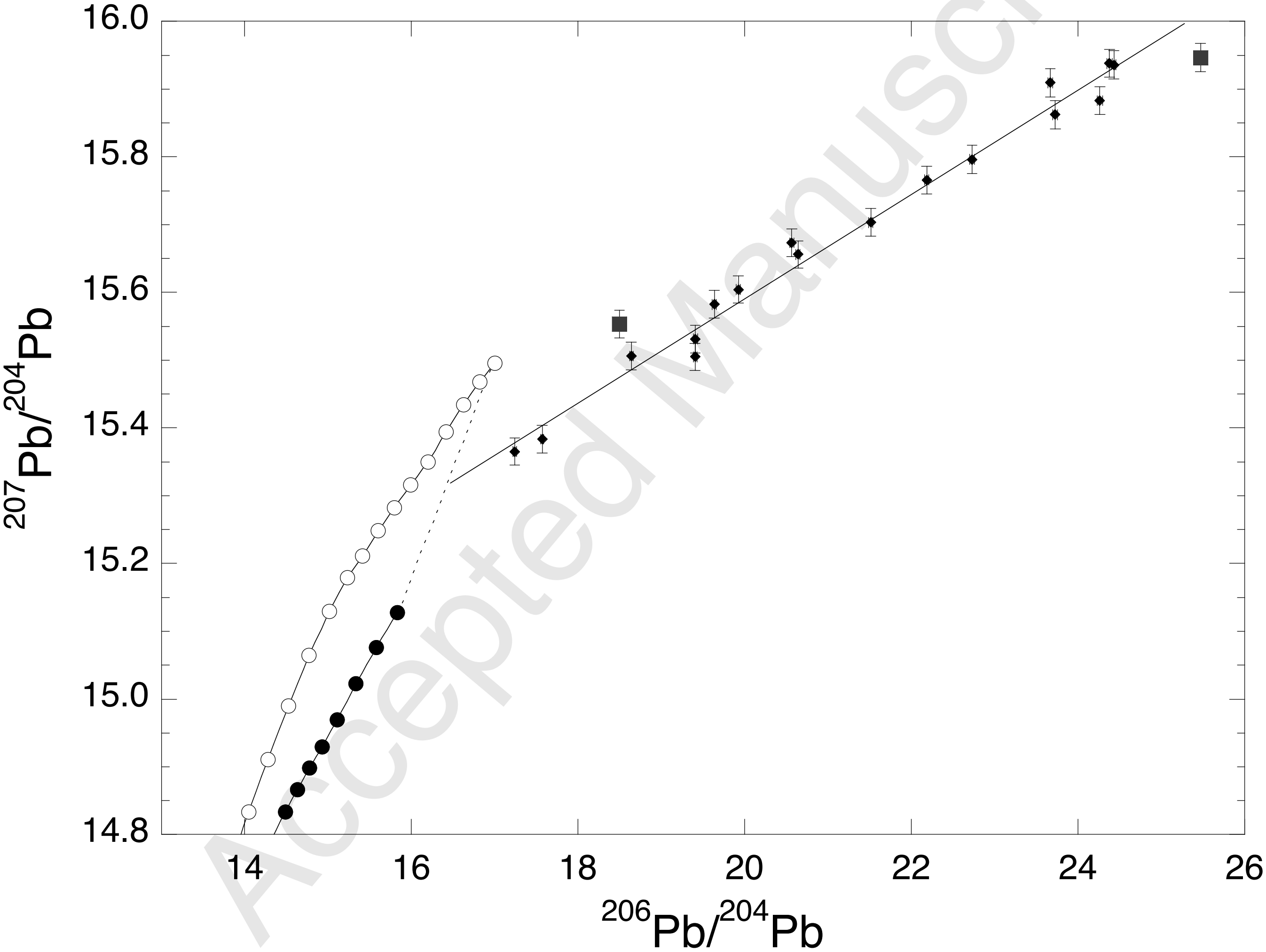
16.0
15.8
15.6
15.4
15.2
15.0
14.8
$^{207}Pb/^{204}Pb$
14
16
18
20
22
24
26
$^{206}Pb/^{204}Pb$

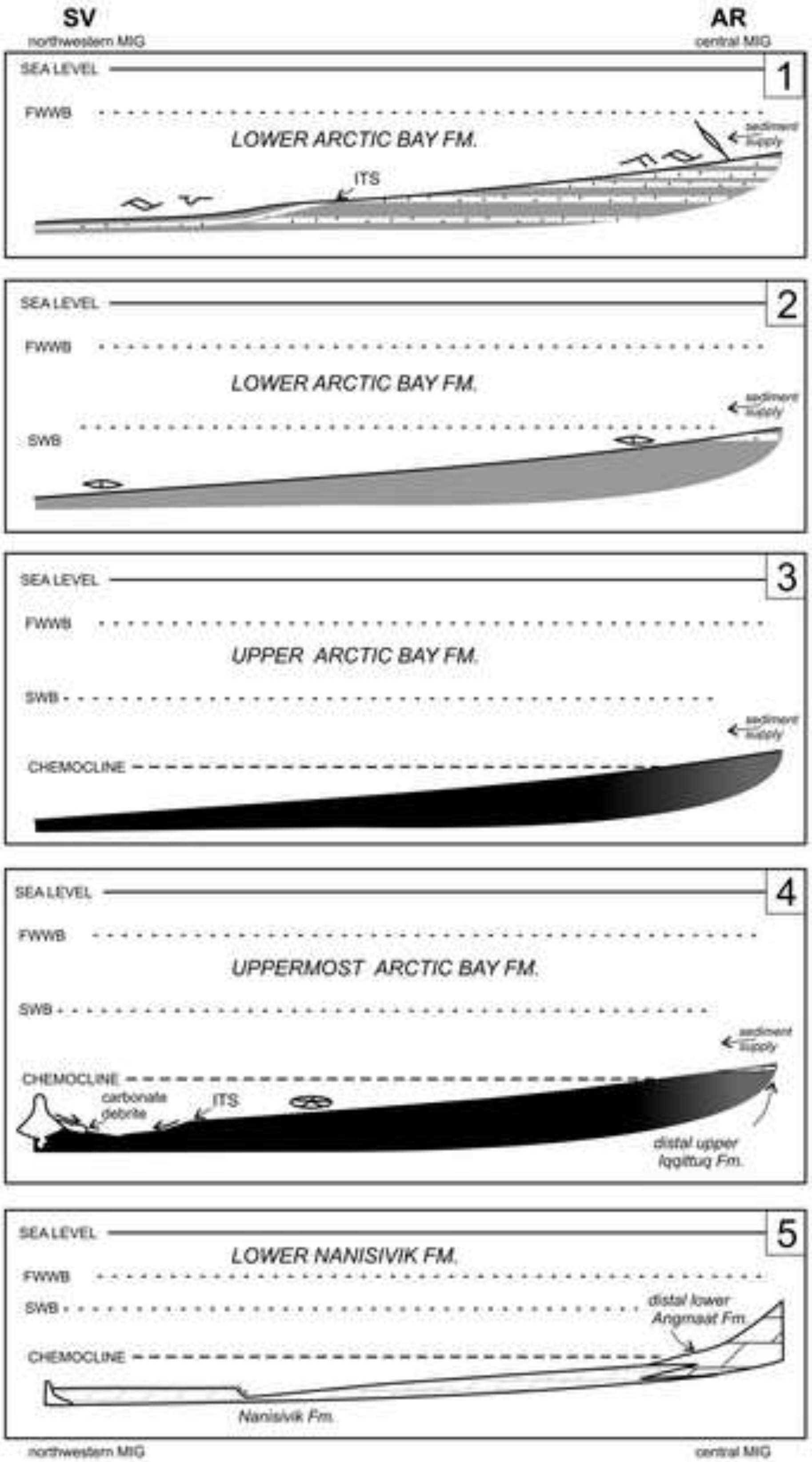
SV
northwestern MIG
AR
central MIG
SEA LEVEL
1
FWWB
LOWER ARCTIC BAY FM.
sediment supply
ITS
SEA LEVEL
2
FWWB
LOWER ARCTIC BAY FM.
sediment supply
SWB
SEA LEVEL
3
FWWB
UPPER ARCTIC BAY FM.
SWB
sediment supply
CHEMOCLINE
SEA LEVEL
4
FWWB
UPPERMOST ARCTIC BAY FM.
SWB
sediment supply
CHEMOCLINE
carbonate debrite
ITS
distal upper Iqqittuq Fm.
SEA LEVEL
5
LOWER NANISIVIK FM.
FWWB
SWB
distal lower Angmaat Fm.
CHEMOCLINE
Nanisivik Fm.
northwestern MIG
central MIG